JOURNAL OF PETROLOGY | VOLUME 44 | NUMBER 6 | PAGES 1055–1075 | 2003

# An Experimentally Constrained Petrogenetic Grid in the Silica-Saturated Portion of the System KFMASH at High Temperatures and Pressures

**KAUSHIK DAS[1]*, SOMNATH DASGUPTA[2] AND HIROYUKI MIURA[1]**

[1]DIVISION OF EARTH AND PLANETARY SCIENCES, GRADUATE SCHOOL OF SCIENCE, HOKKAIDO UNIVERSITY, N10W8, KITA-KU, SAPPORO-SHI, JAPAN, 060-0810

[2]DEPARTMENT OF GEOLOGICAL SCIENCES, JADAVPUR UNIVERSITY, KOLKATA, INDIA

**RECEIVED FEBRUARY 17, 2002; ACCEPTED DECEMBER 6, 2002**

*Experiments in the quartz-saturated part of the system KFMASH under* $fO_2$ *conditions of the haematite–magnetite buffer and using bulk compositions with* $X_{Mg}$ *of 0·81, 0·72, 0·53 define the stability limits of several mineral assemblages within the* P–T *field 9–12 kbar, 850–1100°C. The stability limits of the mineral assemblages orthopyroxene + spinel + cordierite ± sapphirine, orthopyroxene + garnet + sapphirine, sapphirine + cordierite + orthopyroxene and garnet + orthopyroxene + spinel have been delineated on the basis of* P–T *and* T–X *pseudosections. Sapphirine did not appear in the bulk composition of* $X_{Mg} = 0{\cdot}53$*. A partial petrogenetic grid applicable to high Mg–Al granulites metamorphosed at high* $fO_2$*, developed in our earlier work, was extended to higher pressures. The experimental results were successfully applied to several high-grade terranes to estimate* P–T *conditions and retrograde* P–T *trajectories.*

KEY WORDS: *KFMASH equilibria; experimental petrogenetic grid at high* $fO_2$

## INTRODUCTION

Sapphirine-spinel bearing high Mg–Al granulites, potentially derived from biotite dehydration-melting of aluminous pelitic protoliths, provide most convincing evidence for ultrahigh-temperature (>900°C) crustal metamorphism, and allow interpretation of retrograde *P–T* trajectories of granulite terranes [reviewed by Harley (1989, 1998)]. These rocks show evidence of equilibration under both low and high $fO_2$ conditions [near the quartz–fayalite–magnetite (QFM) and nickel–nickel oxide/haematite–magnetite (NNO/HM) buffers, respectively], and theoretical considerations show that significant differences are expected in the topologies of petrogenetic grids in the systems FeO–MgO–$Al_2O_3$–$SiO_2$ (FMAS) (Hensen, 1986) and $K_2O$–FeO–MgO–$Al_2O_3$–$SiO_2$–$H_2O$ (KFMASH) (Hensen & Harley, 1990; Dasgupta *et al.*, 1995) as a result of the effects of variations in $fO_2$ conditions. Primarily the changes in topology are due to the enlarged stability field of spinel + quartz at high $fO_2$ condition leading to grid inversion (Hensen, 1986). As a result, two alternate petrogenetic grids, one for low $fO_2$ and the other for high $fO_2$ conditions, have been customarily used in the systems FMAS and KFMASH (Hensen, 1986; Hensen & Harley, 1990). Experimentally constrained petrogenetic grids are available in the system KFMASH, which successfully explain metamorphic pathways of silica-saturated granulites equilibrated at low $fO_2$ (Audibert *et al.*, 1995; Carrington & Harley, 1995*a*, 1995*b*; Harley, 1998). Experimental data are available in the system FMAS at high $fO_2$ conditions (Annersten & Seifert, 1981), which, however, cannot take into consideration biotite-melting reactions. In a previous publication we developed a theoretical

*Corresponding author. Telephone: +81-11-706-4651. Fax: +81-11-706-4650. E-mail: kaus@ep.sci.hokudai.ac.jp

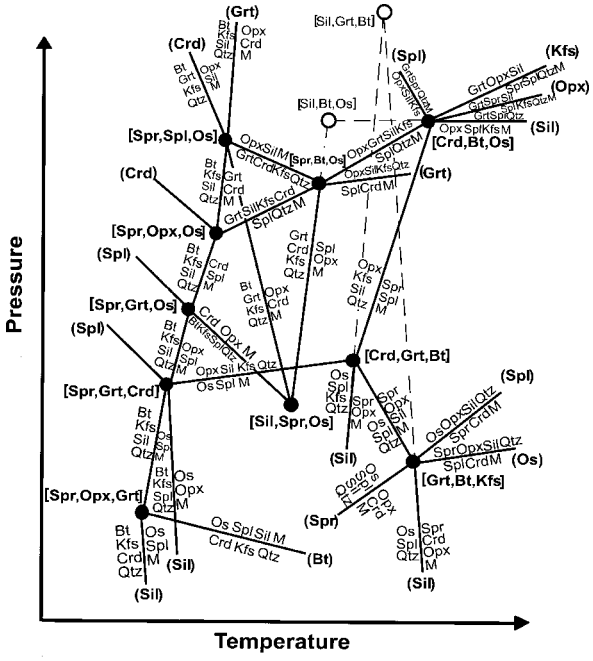


**Fig. 1.** Theoretical $P$–$T$ grid in the silica-saturated portion of the system KFMASH at high $fO_2$ (after Das *et al.*, 2001). ●, stable invariant points; ○, metastable invariant points. Bold lines denote the assumed stable univariant reactions and dashed lines indicate the metastable extension of some stable reactions. Square brackets indicate phases absent from invariant points, whereas curved brackets denote the absent phases in univariant reactions.

petrogenetic grid in the system KFMASH at high $fO_2$ (Fig. 1), justified the choice of stable invariant points in the $n + 3$ multisystem, outlined the scheme to determine slopes of univariant equilibria, discussed the possible roles of non-KFMASH components (Zn in spinel, Na in osumilite, Ti and F in biotite) on the equilibria, and presented a semi-quantitative grid at lower pressures to explain the coexistence of osumilite and spinel in high Mg–Al granulites (Das *et al.*, 2001). In this study, we present an experimentally constrained $P$–$T$ petrogenetic grid in the system KFMASH at high $fO_2$ (HM buffer) at pressures above the stability field of osumilite + spinel, and apply it to several osumilite-free natural assemblages. All mineral abbreviations are after Kretz (1983).

## NATURAL OCCURRENCES AND PREVIOUS EXPERIMENTAL RESULTS AT HIGH $fO_2$

The petrogenetic grids of Carrington & Harley (1995*a*, 1995*b*) and Harley (1998) explain the textural evolution of silica-saturated granulites equilibrated at low $fO_2$, mostly described from East Antarctica and Algeria [references given by Harley (1998)]. These include both osumilite-present and osumilite-absent assemblages. It is intriguing that in the whole range of $P$–$T$, spinel was absent in all the characteristic phase assemblages in these cases. It was argued that spinel-bearing assemblages might be stable at lower pressures. Hensen (1986) showed that owing to the enlargement of the stability field of spinel at high $fO_2$ there is an inversion of the petrogenetic grid in the system FMAS. Consequently, the invariant points [Spr], [Crd] and [Grt] become stable at high $fO_2$, as compared with [Spl], [Opx], [Sil] and [Qtz] stabilized under low $fO_2$ conditions. Combining the low-temperature phase relations of Grant (1985) and high-temperature phase relations of Hensen (1971, 1986), Hensen & Harley (1990) derived a KFMASH petrogenetic grid at low $fO_2$. At high $fO_2$, owing to the extension of the spinel stability field, a new invariant point [Spr,Opx] becomes stable in the system KFMASH (Hensen & Harley, 1990). This results in the stability of the assemblage Spl–Qtz–Bt–melt, which was deemed metastable in the low $fO_2$ grid. Dasgupta *et al.* (1995) used available experimental and natural rock data to position the invariant points [Spr,Opx], [Spr,Bt], [Grt,Bt] and [Crd,Bt] in their high $fO_2$ KFMASH grid in $P$–$T$ space. Together with [Spr,Spl], these invariant points constitute the high-temperature petrogenetic grid in the system KFMASH at high $fO_2$. However, osumilite was not considered in the grids of Hensen & Harley (1990) and Dasgupta *et al.* (1995). Recently, McDade & Harley (2001) proposed a qualitative alternative grid where they considered spinel, but not osumilite, and linked quartz-present and quartz-absent equilibria. In this grid, spinel in the presence of quartz is stable only at less than ~5 kbar but over a wide temperature range. Sapphirine coexists with quartz at very high temperatures and over a wide pressure range. There is a very limited stability field of sapphirine + spinel. Sapphirine + garnet + quartz is stable only at extreme temperatures (approximately >1000°C) and $P$ approximately <8 kbar. The incompatibility of osumilite + spinel, limited stability of spinel + sapphirine, and absence of a stability field for spinel + quartz + orthopyroxene + sillimanite in low $fO_2$ grids are not consistent with many natural assemblages equilibrated at high $fO_2$, as indicated by the common presence of magnetite, ilmenohaematite and haematite. Such assemblages include those of Rogaland (Tobi *et al.*, 1985), Namaqualand (Waters, 1989, 1991; Nowicki *et al.*, 1995), Labwor Hills (Nixon *et al.*, 1973; Sandiford *et al.*, 1987), Wilson Lake (Morse & Talley, 1971), Peekskill, New York (Caporuscio & Morse, 1978), Eastern Labrador (Arima & Gower, 1991) and Eastern Ghats (Grew, 1982; Lal *et al.*, 1987; Kamineni & Rao, 1988; Sengupta *et al.*, 1991; Dasgupta *et al.*, 1995, 1997; Bose *et al.*, 2000).

Annersten & Seifert (1981) have carried out experimental studies at high $fO_2$ in parts of the system FMASHO, and delineated the stability fields of orthopyroxene + sillimanite + quartz, spinel + orthopyroxene + sillimanite + quartz, and cordierite + orthopyroxene + spinel + quartz as functions of bulk-rock $X_{Mg}$ and pressure. The stability field of the key high $fO_2$ FMAS assemblage orthopyroxene + sillimanite + spinel + quartz was delineated in this study. The stability field of spinel is expanded at high $fO_2$ owing to incorporation of $Fe^{3+}$.

Our previously reported experimental data in the system KFMASH at high $fO_2$ (HM buffer) (Das *et al.*, 2001) have shown that: (1) osumilite-bearing assemblages containing spinel solid solutions can appear directly from dehydration-melting of biotite at pressures below 8·5 kbar; (2) at higher temperatures this assemblage gives way to sapphirine-bearing assemblages in highly magnesian bulk compositions; (3) at higher pressures orthopyroxene + sillimanite replaces osumilite + spinel; (4) stability of garnet is enhanced with lowering of bulk-rock mg number. Major differences between the low $fO_2$ (Carrington & Harley, 1995*b*) and high $fO_2$ (Das *et al.*, 2001) phase assemblages in the KFMASH system are: (1) dehydration-melting of biotite at different pressures produces cordierite + orthopyroxene + garnet + melt at low $fO_2$, and osumilite + spinel + orthopyroxene at high $fO_2$; (2) the garnet–osumilite field at low $fO_2$ is replaced by the osumilite–spinel field at high $fO_2$; (3) garnet-bearing assemblages become unstable at higher pressures at low $fO_2$, but these become stable at high $fO_2$ at higher pressures. Here, we present further experimental assemblage data for the $P$–$T$ range 8·5–12 kbar and 800–1100°C, quantify the theoretical grid within this $P$–$T$ window, and apply it to some natural mineral assemblages. Only some of the invariant points shown in Fig. 1 will be accessible to particular bulk compositions within the $P$–$T$ range of the experiments.

## EXPERIMENTAL PROCEDURE

Details of the experimental procedure, synthesis of starting material and its composition have been given by Das *et al.* (2001). However, the salient points are repeated below. The experiments were carried out using synthetic and natural mineral mixtures as starting materials. The experimental mixtures contained synthetic biotite, K-feldspar, quartz and an aluminosilicate gel of the composition 80% sillimanite + 20% quartz. Gels for synthesis of biotite and K-feldspar were prepared following the procedure of Iiyama *et al.* (1994). Biotite and K-feldspar were synthesized in a hydrothermal apparatus. For biotite a reduced KFMASH gel was pressed at 2 kbar and 750°C. A double-capsule technique was employed for synthesis runs, with an inner $Ag_{70}$–$Pd_{30}$ sealed capsule containing the charge and an outer gold capsule containing iron–wüstite solid buffer. As the buffer reacts out faster than the charge, the run was quenched every 2 days, and the buffer mixture was changed, keeping the inner capsule intact. The total length of each run was 7 days, which produced single-phase biotite that was confirmed by powder X-ray diffraction (XRD) and analysed by electron probe microanalysis (EPMA). K-feldspar was synthesized from KAS gel at 2 kbar and 700°C for a week in a hydrothermal vessel. Reactions involving natural sillimanite reportedly being slow, a gel with composition of 80% sillimanite and 20% quartz was used in the mineral mixtures. Natural sillimanite and garnet (pyrope–almandine–grossular solid solution) crystals were used as seeds. The garnet seed is from granulites from Antarctica (sample from Hokkaido University Museum) and sillimanite is from a high-grade gneiss from South Africa (Nichika Company, Japan). Synthetic quartz crystals prepared from Brazilian quartz (LASCA) by Fine Crystals Pvt. Ltd, Japan, were used in the final mixtures. Synthetic minerals and gels (dried in a conventional furnace at 600°C for 24 h and then kept in an oven at 120°C) were mixed with natural garnet and sillimanite crystals in three different proportions to obtain mixtures of three different quartz-saturated bulk compositions. These differed only in Mg:Fe ratios (as the synthetic biotite had three different Mg:Fe ratios), and are labelled as M1 ($X_{Mg} = 0{\cdot}81$), M2 ($X_{Mg} = 0{\cdot}72$), and M3 ($X_{Mg} = 0{\cdot}53$). These mixtures were ground under acetone to nearly 10 mm sieve size and kept in an oven at 120°C.

These dry mineral mixtures were used as charges in sealed $Ag_{70}$–$Pd_{30}$ capsules. To control the oxygen partial pressure in the cell, a double-capsule technique was used, with an outer capsule of Pt containing the sealed $Ag_{70}$–$Pd_{30}$ inner capsule and packed with solid haematite–magnetite powder. Although a drop of water is used in the solid buffer mixture in the outer capsule, the inner capsule contained only dry mineral mixtures and hence the experiments were carried out under vapour-absent conditions. The sealed double capsule was placed in a $\frac{1}{2}$ inch talc–Pyrex glass cell assembly and pressed in a Boyd & England (1960) type piston-cylinder apparatus. After each run, upon puncturing the outer capsule the audible hissing sound or observed bubbling through the water droplet at the puncture indicated the presence of water and/or a gas phase in the buffer mixture. The presence of powder XRD peaks of both haematite and magnetite in the product buffer material indicated the persistence of buffer. It is therefore assumed that the oxygen fugacity was buffered at or near the HM buffer curve. Any possible contamination in the inner capsule was checked

by weighing it before and after the runs. The temperature was measured by alumel–chromel thermocouples at temperatures lower than 1050°C and Pt–Rh13% at temperature higher than 1050°C. No e.m.f. correction was employed. Pressure calibration runs for the double-capsule cell assembly were carried out using quartz and coesite. Haematite and magnetite powder mixture was used to prevent the entry of hydrogen in the inner capsule. The quartz–coesite phase transition data of Bohlen & Boettcher (1982) were followed. We carried out pressure calibration runs both before and after the main experiments. We have further checked the results with the melting curves of LiCl and NaCl at 10 kbar after the data of Clarke (1959). Both the results indicate a pressure correction of nearly –13% with our cell design. With the similar talc–Pyrex cell in the same apparatus, Hariya & Fukunaga (1969) reported a pressure correction of nearly –10%. As they performed the calibration experiment with a single-capsule design, our calibration results appear to be more acceptable, with a slightly more resistive double-capsule cell. Pressure and temperature became stable within the first 1–2 h of each run. The estimated temperature and pressure uncertainties are ±5°C and ±0·2–0·3 kbar, respectively.

The inner capsule was opened after weighing, and part of the quenched sample was used for XRD measurement. Thin sections were prepared for optical microscopic study, for taking backscattered electron (BSE) images, and for analysis by EPMA. Although powder XRD patterns were taken for most of the samples, some of the samples were checked with micro-area XRD with 50 and 100 μm collimeters. An accelerating voltage of 15 kV and a current of 20 nA were used while analysing with a JEOL733 electron microprobe. The melt phase was analysed using different beam sizes (5–15 μm), counting times (10–20 s), and beam currents (7–20 nA). The loss in potassium count has been studied by plotting the count against time, beam size, and beam current. Minimum potassium count loss was observed when a 15 μm beam with 15 nA current was used for 10 s.

Reversal was attempted for some critical univariant reactions. A two-stage technique after Carrington & Harley (1995*a*) was employed. In most of the long duration reversal runs, either the buffer was exhausted or the capsule burst. We succeeded in only three reversal runs for the reactions Opx + Sil + Kfs + Qtz = Spr + Spl + L (Crd, Grt, Bt, Os); Os + Spl + L = Opx + Sil + Kfa + Qtz (Spr, Grt, Crd, Bt), and Os + Spl + Qtz = Spr + Crd + Opx + L (Grt, Bt, Kfs, Sil), where there was a distinct change in the modal abundance of the phases when approached from either side.

Reversal runs across univariant reaction boundaries, chemical homogeneity of the product phases, and consistent element partitioning between coexisting phases are the criteria used in the present experiments to infer approach to chemical equilibrium. Further details have been given by Das *et al.* (2001) regarding testing of equilibrium and of the nature of the run products.

Table 1 lists the experimental conditions and run products obtained from the three bulk compositions within the $P$–$T$ interval 9–12 kbar, 850–1100°C.

## CHEMISTRY OF THE PRODUCT PHASES

### Cordierite

Synthetic cordierite varies in $X_{Mg}$ from 0·9–0·96 for the M1 bulk composition to 0·84–0·94 for M2 and to 0·81–0·87 for M3 bulk compositions. Very little $Fe^{3+}$ is suspected to be present on the basis of stoichiometry. Cation totals exceed 11 on a 10-oxygen basis as a result of the presence of a small amount of potassium, which was also found by Carrington & Harley (1995*a*) in their runs. In most of the runs, cordierite was grown as large euhedral crystals of 10–50 μm.

### Orthopyroxene

Orthopyroxene formed always as large elongated (10–30 μm length and 10–15 μm width) crystals of remarkably homogeneous composition (Table 2). The $X_{Mg}$ varies from 0·83–0·90 for the M1 bulk composition to 0·78–0·89 for M2 and 0·69–0·85 for the M3 bulk composition. Orthopyroxene is highly aluminous, presumably because of the use of $sillimanite_{80}$–$qtz_{20}$ gel in the starting material. The A/AFM values range from 0·10 to 0·15 with the maximum data concentration in the range 0·11–0·13. We have plotted the $Al_2O_3$ content of synthetic orthopyroxene (coexisting with Grt, Spr, Sil, Kfs, Liquid with or without Spl) as a function of temperature in Fig. 2. In accordance with the observations of Harley (1998) and Harley & Motoyoshi (2000) we observe a positive correlation. It is also clear that with increasing iron in the bulk composition (as well as in orthopyroxene, as mentioned above) the A/AFM parameter increases, as also observed in earlier experimental studies (Arima, 1978; Annersten & Seifert, 1981; Harley, 1984). Moreover, Arima (1978) and Annersten & Seifert (1981) showed that the $Fe^{3+}$ content, i.e. the ferritschermak component, also increases with increasing iron in the bulk composition at high $fO_2$. As some of the synthetic orthopyroxene compositions are slightly non-stoichiometric, we did not attempt to recalculate $Fe^{3+}$.

### Sapphirine

Sapphirine is present in runs with mixtures M1 and M2 within the $P$–$T$ range. Sapphirine composition has

*Table 1: Experimental run conditions and product phases*

| Bulk | $P$ (kbar) | $T$ (°C) | Time (h) | Product phases (major) | Product phases (minor) |
|---|---|---|---|---|---|
| M1 | 9 | 850 | 188 | Bt, Sil, Qtz, Kfs | Opx(0·88), L |
| M1 | 9 | 900 | 240 | Qtz, Opx(0·89), Sil, L | Kfs, Spl |
| M1 | 9 | 1000 | 240 | Opx(0·76), Kfs, Qtz, L | Spr(0·9), Spl |
| M1 | 9 | 1050 | 212 | L, Opx(0·83), Spr(0·85) | Qtz, Sil |
| M1 | 9 | 1100 | 212 | L, Spr(0·94), Opx(0·91) | Crd(0·94), Qtz, Spl(0·53) |
| M1 | 10 | 900 | 222 | Opx(0·87), Qtz, Kfs | Spl, L, Bt |
| M1 | 10 | 965 | 228 | Opx(0·81), Qtz, L, Sil | Grt(0·5), Kfs |
| M1 | 10 | 1000 | 168 | Opx(0·83), Qtz, Sil, L | Kfs, Spl |
| M1 | 10 | 1050 | 144 | Qtz, Spr(0·87), Sil, L, Opx(0·9) | Kfs, Spl(0·58) |
| M1 | 10 | 1100 | 168 | Opx(0·86), L, Spr(0·79), Grt(0·62), Spl | Qtz, Kfs |
| M1 | 11 | 800 | 238 | Qtz, Kfs, Sil, Bt | L |
| M1 | 11 | 900 | 240 | Qtz, Opx(0·85), Bt, Kfs | L |
| M1 | 11 | 1000 | 241 | Qtz, Opx(0·83), Sil, Grt(0·58), L | Kfs |
| M1 | 11 | 1050 | 240 | Grt(0·54), Qtz, Kfs, Opx(0·86), L | Spr(0·85), Sil |
| M1 | 11 | 1100 | 242 | Opx(0·87), Qtz, L, Sil | Grt(0·51), Spr(0·88) |
| M1 | 12 | ~850?* | 245 | Bt, Qtz, Sil, Kfs | L |
| M1 | 12 | 900 | 240 | Opx(0·86), Bt, Kfs, Qtz, L | Grt(0·7), Sil |
| M1 | 12 | 1000 | 192 | Opx(0·90), Sil, Qtz, L, Kfs | Grt(0·56) |
| M1 | 12 | 1050 | 192 | L, Opx(0·88), Grt(0·8), Sil, Qtz | Spr |
| M2 | 8·5 | 950 | 240 | Opx, Qtz, Kfs, L | Sil, Spl(0·5) |
| M2 | 8·5 | 1050 | 212 | Opx(0·82), Spl(0·59), L, Spr(0·85), Qtz | Crd(0·92) |
| M2 | 9 | 850 | 188 | Bt, Sil, Qtz, Kfs | L |
| M2 | 9 | 900 | 212 | Qtz, Opx(0·88), L | Bt, Kfs, Spl |
| M2 | 9 | 1000 | 200 | Opx(0·83), Sil, Qtz, L | Spl(0·6), Grt(0·58), Kfs |
| M2 | 9 | 1100 | 188 | L, Spr(0·92), Spl(0·56), Opx(0·83) | Qtz |
| M2 | 10 | 900 | 222 | Bt, Opx(0·86), L, Qtz, Sil | Spl(0·63), Kfs |
| M2 | 10 | 1000 | 168 | Opx(0·87), Qtz, L | Spl(0·7), Grt |
| M2 | 10 | 1100 | 144 | Spr(0·86), Opx(0·83), L | Qtz, Grt(0·52) |
| M2 | 11 | 850 | 240 | Bt, Qtz, Kfs, Sil | |
| M2 | 11 | 950 | 212 | Opx(0·86), Grt(0·52), Qtz | Spl, L |
| M2 | 11 | 1050 | 168 | Grt(0·55), Opx(0·84), L, Qtz | Spr(0·84), Kfs |
| M3 | 9 | 800 | 228 | Bt, Qtz, Grt(seed), Kfs | L |
| M3 | 9 | 900 | 212 | Opx(0·84), Spl(0·3), L, Kfs | Qtz, Sil |
| M3 | 9 | 965 | 188 | Opx (0·75), Sil, Spl(0·52), Qtz, L | Grt(0·46), Kfs |
| M3 | 9 | 1000 | 200 | Opx(0·7), L, Sil, Grt(0·58) | Qtz, Kfs |
| M3 | 9 | 1100 | 212 | L, Spl(0·51), Crd(0·89), Opx(0·87) | Qtz |
| M3 | 9·5 | 1000 | 168 | Grt(0·6), Opx(0·7), Qtz, L | Sil |
| M3 | 10 | 850 | 240 | Bt, Opx(0·74), Spl(0·46), Qtz | L, Sil, Kfs |
| M3 | 10 | 900 | 230 | Opx(0·7), L, Qtz, Grt(0·59) | Sil |
| M3 | 10 | 1100 | 144 | L, Qtz, Spl(0·54), Opx(0·74) | Grt(0·48), Sil, Kfs |
| M3 | 11 | 850 | 212 | Qtz, Bt, Kfs, Opx(0·75), Sil | L |
| M3 | 11 | 900 | 212 | Qtz, Opx(0·71), Kfs, L | Grt(0·58) |
| M3 | 11 | 1000 | 188 | L, Opx(0·72), Spl(0·56), Qtz, Grt(0·48) | Sil |

The first column on the left indicates the bulk compositions as in the text. Values in parentheses indicate the $X_{Mg}$ of the phases. Major and minor products have been divided on the approximate modal abundance (approximately $<10\%$ as minor product and $>10\%$ as major product) as observed under optical microscope. Reversal runs were carried out at 9 kbar from 950°C to 1050°C at every 25°C. It was found that the modal proportion of sapphirine and spinel increases with rising temperature. With M1 mix, sapphirine first appeared at 975°C.
*Thermocouple failed after 96 h.

*Table 2: Representative chemical analysis of orthopyroxene*

| Bulk: | M1 | | | | M2 | | | | M3 | | | | | |
|---|---|---|---|---|---|---|---|---|---|---|---|---|---|---|
| *P* (kbar): | 9 | 10 | 11 | 12 | 10 | 9 | 11 | 9 | 9 | 9 | 10 | 10 | 11 | 11 |
| *T* (°C): | 900 | 1050 | 1100 | 1000 | 900 | 900 | 1050 | 1000 | 900 | 1000 | 900 | 1100 | 850 | 1000 |
| *n*: | 3 | 5 | 5 | 4 | 4 | 3 | 5 | 3 | 4 | 5 | 4 | 5 | 3 | 5 |
| $SiO_2$ | 51·52 | 51·23 | 50·88 | 51·30 | 50·52 | 49·80 | 50·40 | 50·55 | 49·14 | 47·96 | 50·48 | 49·75 | 53·00 | 47·69 |
| $Al_2O_3$ | 11·72 | 12·28 | 13·08 | 12·35 | 10·71 | 11·36 | 12·13 | 12·18 | 11·71 | 13·87 | 10·46 | 12·85 | 10·73 | 13·22 |
| FeO | 6·33 | 5·45 | 7·36 | 6·36 | 8·78 | 8·78 | 9·04 | 9·97 | 10·63 | 16·47 | 17·34 | 14·71 | 13·34 | 16·29 |
| MgO | 29·97 | 30·41 | 27·88 | 29·98 | 29·45 | 29·59 | 27·57 | 27·03 | 27·94 | 22·66 | 22·41 | 22·87 | 21·80 | 23·38 |
| CaO | 0·02 | 0·02 | 0·02 | 0·04 | 0·02 | 0·00 | 0·02 | 0·06 | 0·02 | 0·01 | 0·01 | 0·03 | 0·12 | 0·01 |
| $K_2O$ | 0·00 | 0·00 | 0·04 | 0·00 | 0·00 | 0·00 | 0·10 | 0·03 | 0·00 | 0·00 | 0·09 | 0·16 | 0·19 | 0·00 |
| $Na_2O$ | 0·03 | 0·07 | 0·01 | 0·00 | 0·01 | 0·01 | 0·00 | 0·02 | 0·02 | 0·01 | 0·00 | 0·02 | 0·03 | 0·00 |
| Total | 99·59 | 99·46 | 99·28 | 100·02 | 99·49 | 99·52 | 99·26 | 99·83 | 99·46 | 100·98 | 100·79 | 100·40 | 99·22 | 100·59 |
| Si | 1·779 | 1·765 | 1·768 | 1·764 | 1·770 | 1·746 | 1·769 | 1·770 | 1·739 | 1·713 | 1·809 | 1·769 | 1·883 | 1·711 |
| Al(T) | 0·221 | 0·235 | 0·232 | 0·236 | 0·230 | 0·254 | 0·231 | 0·230 | 0·261 | 0·287 | 0·191 | 0·231 | 0·117 | 0·289 |
| $\sum$ | 2·000 | 2·000 | 2·000 | 2·000 | 2·000 | 2·000 | 2·000 | 2·000 | 2·000 | 2·000 | 2·000 | 2·000 | 2·000 | 2·000 |
| Al(O) | 0·256 | 0·264 | 0·304 | 0·265 | 0·212 | 0·215 | 0·270 | 0·273 | 0·227 | 0·296 | 0·251 | 0·307 | 0·332 | 0·270 |
| $Fe^{3+}$ | 0·000 | 0·000 | 0·000 | 0·000 | 0·018 | 0·039 | 0·000 | 0·000 | 0·034 | 0·000 | 0·000 | 0·000 | 0·000 | 0·019 |
| $Fe^{2+}$ | 0·183 | 0·157 | 0·214 | 0·183 | 0·232 | 0·200 | 0·265 | 0·292 | 0·265 | 0·492 | 0·520 | 0·437 | 0·396 | 0·461 |
| Mg | 1·542 | 1·562 | 1·444 | 1·537 | 1·538 | 1·546 | 1·442 | 1·411 | 1·473 | 1·206 | 1·197 | 1·212 | 1·154 | 1·250 |
| $\sum$ | 1·981 | 1·983 | 1·962 | 1·985 | 2·000 | 2·000 | 1·977 | 1·976 | 1·999 | 1·994 | 1·968 | 1·956 | 1·882 | 2·000 |
| Ca | 0·001 | 0·001 | 0·001 | 0·001 | 0·001 | 0·000 | 0·001 | 0·002 | 0·001 | 0·000 | 0·000 | 0·001 | 0·005 | 0·000 |
| Na | 0·002 | 0·005 | 0·001 | 0·000 | 0·000 | 0·000 | 0·000 | 0·002 | 0·001 | 0·001 | 0·000 | 0·001 | 0·002 | 0·000 |
| K | 0·000 | 0·000 | 0·002 | 0·000 | 0·000 | 0·000 | 0·004 | 0·001 | 0·000 | 0·000 | 0·004 | 0·007 | 0·009 | 0·000 |
| $\sum$ | 1·984 | 1·989 | 1·965 | 1·986 | 2·001 | 2·000 | 1·982 | 1·981 | 2·001 | 1·995 | 1·972 | 1·965 | 1·898 | 2·000 |
| Total | 3·984 | 3·989 | 3·965 | 3·986 | 4·001 | 4·000 | 3·982 | 3·981 | 4·001 | 3·995 | 3·972 | 3·966 | 3·898 | 4·000 |
| $X_{Mg}$ | 0·894 | 0·909 | 0·871 | 0·894 | 0·869 | 0·886 | 0·845 | 0·829 | 0·847 | 0·710 | 0·697 | 0·735 | 0·745 | 0·731 |

Oxygen basis is six. *n*, number of point analysis. These analyses are included to illustrate the variation in composition and not the stoichiometry.

been recalculated according to the scheme of Higgins *et al.* (1979), and the $Fe^{3+}/Fe^{2+}$ ratio has been calculated from charge balance criteria. The compositional data (Table 3), when plotted in (FeO + MgO)–($Al_2O_3$ + $Fe_2O_3$)–$SiO_2$ compositional space (Fig. 3), show that most fall between 7:9:3 and 2:2:1 compositions, but mostly very close to 2:2:1. However, some of the grains are slightly silicic and non-stoichiometric, which renders recalculation of $Fe^{3+}$ difficult. This is a problem commonly encountered in the high-temperature–high-pressure synthetic experiments where seed crystals are not used (Hensen & Green, 1971; Newton, 1972). Again, some less silicic sapphirine plots outside the ideal substitution line between 7:9:3 and 2:2:1 (Fig. 3). This is probably due to incorrect estimation of $Fe^{3+}$, as also observed by Waters (1986). The $X_{Mg}$ [= Mg/(Mg + $Fe^{2+}$)] of sapphirine in the M1 bulk composition ranges between 0·8 and 0·91, and that for the M2 bulk composition between 0·82 and 0·86. Normally, sapphirine occurs as small stubby grains (10–20 μm) in the run products (Fig. 4a).

## Garnet

In some shorter duration runs, new garnet forms as rims on seed crystals (Fig. 4b), which are compositionally distinct, and therefore failed to equilibrate. In most of the runs of longer duration, garnet formed as new crystals of remarkably homogeneous composition. The garnet seeds (almandine–pyrope–grossular) used in the experiment have low grossular component (3·6 wt % of CaO). The minor grossular content of the homogeneous garnets (maximum 0·79 mol %) is surprising, and is possibly residual from the seed

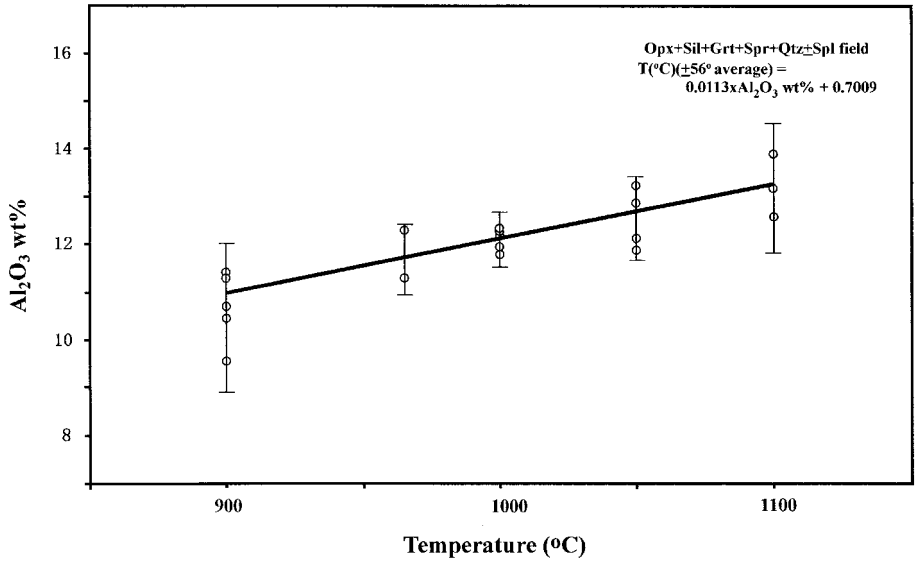


**Fig. 2.** Alumina content in synthetic orthopyroxene ($Al_2O_3$ wt %) plotted against temperature.

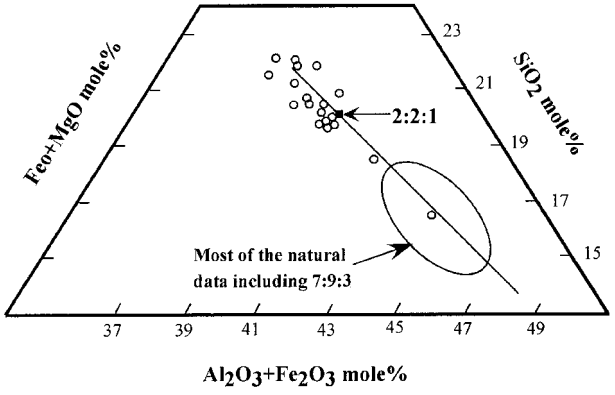


**Fig. 3.** Chemical composition of synthetic sapphirine plotted in (FeO + MgO)–($Al_2O_3$ + $Fe_2O_3$)–$SiO_2$ compositional space. It should be noted that most of the sapphirines are close to the composition 2:2:1 with some intermediate between 2:2:1 and 7:9:3.

(Carrington & Harley, 1995*a*). $X_{Mg}$ [= Mg/(Mg + Fe)] varies between 0·45 and 0·65 (Table 4). New garnet was produced at high pressures even at temperatures as low as 900°C for the M3 bulk composition in long duration runs (Table 1). Therefore, we believe that for short duration runs there was a kinetic problem of garnet growth, but not for long duration runs where equilibrium was attained.

## Spinel

Spinel forms euhedral grains $<15\,\mu m$ in diameter. Recalculation of analytical data (Table 4) on the basis of charge balance criteria shows a significant amount of $Fe^{3+}$ in spinel. The $Fe^{3+}$/Fe(total) ratio varies between 0·07 and 0·54. Spinel is the most iron-rich phase in low-pressure runs where garnet is absent. $X_{Mg}$ varies in the range 0·41–0·58, 0·40–0·54 and 0·32–0·5 in the M1, M2 and M3 bulk compositions, respectively.

## Sillimanite

Sillimanite contains very minor $Fe^{3+}$ (0·008–0·035 cations per formula unit) (Table 4).

## Melt

In runs below 950°C the amount of melt produced was very small. The analytical data for the melt phase show very minor amounts of FeO and MgO in total not exceeding 2·5 wt % (Table 5). Moreover, because of the presence of undetectable fine grains of some solid phases in the glass pool, it has been previously suggested that there is a possibility of contamination (Audibert *et al.*, 1995). The ferrous:ferric ratio of the glass from the present experiments could not be determined. When plotted in an AKM diagram, the present data concentrate very close to the composition that approximates glass with minimum contamination (Audibert *et al.*, 1995). Moreover, normative calculations (ignoring iron and magnesium) of our data suggest a trend in the direction of increasing normative quartz and corundum, which is possibly due to potassium loss during the analysis (Fig. 5). Despite the uncertainties, the melt composition obtained in the present experiments is strikingly similar to that

*Table 3: Representative chemical analyses of sapphirine*

| Bulk: | M1 | | | | M2 | | |
|---|---|---|---|---|---|---|---|
| *P* (kbar): | 9 | 10 | 10 | 11 | 8·5 | 10 | 11 |
| *T* (°C): | 1000 | 1100 | 1050 | 1100 | 1050 | 1100 | 1050 |
| *n*: | 4 | 2 | 5 | 4 | 5 | 5 | 4 |
| $SiO_2$ | 18·51 | 15·15 | 16·96 | 17·46 | 16·92 | 16·79 | 16·69 |
| $Al_2O_3$ | 55·77 | 55·99 | 55·29 | 57·64 | 55·97 | 55·96 | 55·03 |
| FeO | 4·02 | 11·43 | 5·70 | 5·06 | 7·68 | 7·11 | 8·64 |
| MgO | 19·96 | 16·91 | 19·33 | 18·45 | 20·13 | 19·55 | 19·35 |
| CaO | 0·00 | 0·05 | 0·00 | 0·00 | 0·01 | 0·00 | 0·01 |
| $K_2O$ | 0·19 | 0·22 | 0·00 | 0·09 | 0·00 | 0·00 | 0·00 |
| $Na_2O$ | 0·00 | 0·00 | 0·02 | 0·03 | 0·00 | 0·00 | 0·00 |
| Total | 98·45 | 99·76 | 97·30 | 98·72 | 100·71 | 99·41 | 99·71 |
| Si | 2·19 | 1·85 | 2·05 | 2·07 | 2·00 | 2·00 | 2·00 |
| Al-T | 3·81 | 4·15 | 3·95 | 3·93 | 4·00 | 4·00 | 4·00 |
| $\sum$ | 6·00 | 6·00 | 6·00 | 6·00 | 6·00 | 6·00 | 6·00 |
| Al-O | 3·98 | 3·88 | 3·94 | 4·13 | 3·80 | 3·87 | 3·78 |
| $Fe^{3+}$ | 0·00 | 0·27 | 0·01 | 0·00 | 0·20 | 0·12 | 0·22 |
| $\sum$ | 3·98 | 4·15 | 3·95 | 4·13 | 4·00 | 4·00 | 4·00 |
| $Fe^{2+}$ | 0·40 | 0·89 | 0·57 | 0·50 | 0·55 | 0·59 | 0·65 |
| Mg | 3·52 | 3·07 | 3·49 | 3·26 | 3·55 | 3·48 | 3·46 |
| $\sum$ | 3·92 | 3·96 | 4·05 | 3·76 | 4·10 | 4·06 | 4·11 |
| Ca | 0·00 | 0·01 | 0·00 | 0·00 | 0·00 | 0·00 | 0·00 |
| Na | 0·00 | 0·00 | 0·00 | 0·01 | 0·00 | 0·00 | 0·00 |
| K | 0·03 | 0·03 | 0·00 | 0·01 | 0·00 | 0·00 | 0·00 |
| $\sum$ | 0·03 | 0·04 | 0·00 | 0·02 | 0·00 | 0·00 | 0·00 |
| Total | 13·93 | 14·15 | 14·01 | 13·91 | 14·10 | 14·06 | 14·11 |
| $X_{Mg}$ | 0·90 | 0·78 | 0·86 | 0·87 | 0·86 | 0·86 | 0·84 |
| $Fe^{3+}/Fe(T)$ | 0·00 | 0·24 | 0·02 | 0·00 | 0·27 | 0·17 | 0·25 |

Oxygen basis is 20. *n*, number of point analysis. These analyses are included to illustrate the variation in composition and not the stoichiometry.

obtained in other experiments (Carrington & Harley, 1995*a*) and in natural occurrences (Patiño Douce & Johnston, 1991).

As osumilite was not produced in our higher-pressure experiments the compositional characteristics of synthetic osumilite are given by Das *et al.* (2001).

The $X_{Mg}$ values of the phases decrease in the order Crd > Os > Spr > Opx > Spl > Grt consistent with Ellis *et al.* (1980). Compositions of coexisting phases obtained at 10 kbar, 1100°C are plotted in $(Al_2O_3)$–$(FeO + MgO)$–$(SiO_2)$ space projected from quartz, K-feldspar and melt in Fig. 6a. In Fig. 6b the same phases are plotted after correcting for $Fe^{3+}$ in $(Al_2O_3 + Fe_2O_3)$–$(MgO + FeO)$–$(SiO_2)$ space. This results in a considerable shift in the position of spinel. This aspect is discussed further in the next section. McDade & Harley (2001) emphasized the importance of using the correct melt composition for projection. We have used the analysed melt composition of the particular run to project the composition of the phases in these plots (Fig. 6a and b).

## Fe–Mg distribution in the coexisting phases

Distribution of Fe–Mg between coexisting garnet–orthopyroxene, spinel–cordierite and sapphirine–spinel as a function of temperature was determined from the analytical data. In coexisting osumilite–cordierite, the latter is slightly more magnesian, similar to that in natural occurrences equilibrated at high $fO_2$ (Das *et al.*, 2001).

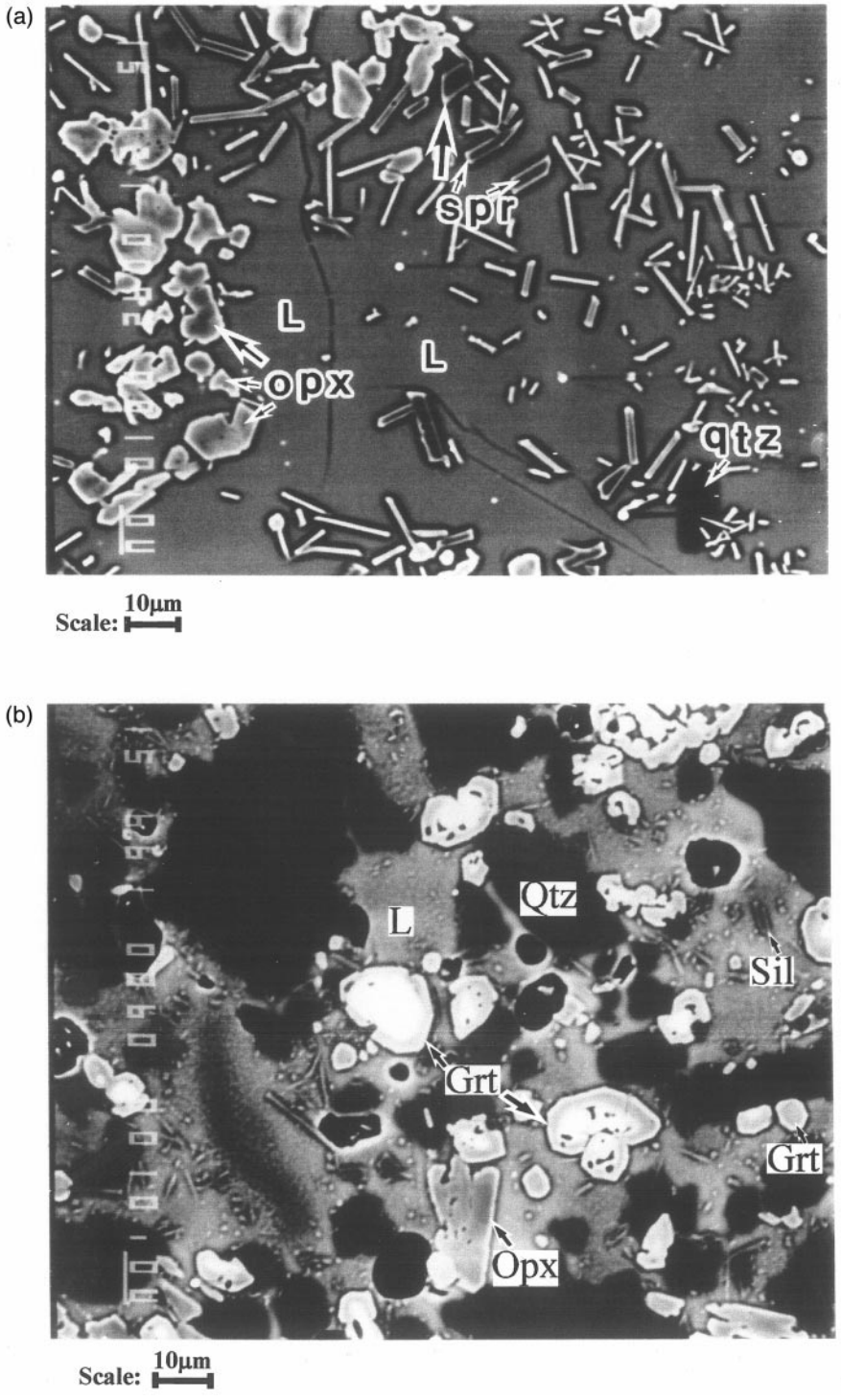


**Fig. 4.** (a) BSE image of the run product at 9 kbar, 1050°C for M1 bulk composition showing synthetic sapphirine. (b) BSE image of the run product at 12 kbar, 1000°C for M1 bulk composition showing new garnet growth on seed crystals. Mineral abbreviations are as in the text.

Figure 7a shows a plot of ln $K_D$ (garnet–orthopyroxene) against temperature, and for comparison the calibrations of Harley (1984) and Lee & Ganguly (1988) have been also plotted. Although many of the data are within the uncertainty limits of the calibration by Lee & Ganguly (1988), there is a scatter of data. The scatter is mainly due to heterogeneous garnet compositions, obtained in shorter duration runs. Similar

*Table 4: Representative chemical data of garnet, spinel and sillimanite*

| Bulk: | M1 | M1 | M2 | M2 | M3 | M3 | | M1 | M2 | M2 | M3 | M3 | | M1 | M1 | M2 | M2 | M3 |
|---|---|---|---|---|---|---|---|---|---|---|---|---|---|---|---|---|---|---|
| *P* (kbar): | 11 | 11 | 11 | 11 | 10 | 11 | | 10 | 9 | 9 | 9 | 10 | | 10 | 10 | 9 | 10 | 9 |
| *T* (°C): | 1000 | 1100 | 950 | 1050 | 1100 | 1000 | | 1050 | 1000 | 1100 | 1100 | 850 | | 965 | 1050 | 1000 | 900 | 1000 |
| *n*: | 5 | 3 | 6 | 5 | 3 | 4 | | 3 | 2 | 6 | 6 | 3 | | 4 | 6 | 5 | 4 | 5 |
| $SiO_2$ | 41·32 | 40·88 | 40·45 | 40·87 | 39·11 | 39·67 | $SiO_2$ | 1·80 | 0·13 | 1·63 | 0·12 | 1·23 | $SiO_2$ | 40·31 | 37·89 | 37·76 | 40·09 | 37·10 |
| $Al_2O_3$ | 23·29 | 23·14 | 22·82 | 23·21 | 21·94 | 22·17 | $Al_2O_3$ | 58·33 | 58·28 | 58·51 | 41·97 | 44·20 | $Al_2O_3$ | 58·06 | 61·95 | 61·84 | 59·97 | 60·21 |
| FeO | 19·81 | 22·77 | 22·27 | 21·13 | 25·45 | 24·40 | $Fe_2O_3$ | 5·09 | 8·15 | 4·37 | 24·81 | 21·36 | FeO | 1·55 | 0·29 | 0·55 | 0·36 | 2·69 |
| MgO | 14·97 | 13·28 | 13·62 | 15·06 | 12·92 | 12·84 | FeO | 19·89 | 17·97 | 21·40 | 20·71 | 23·73 | MgO | 0·23 | 0·06 | 0·10 | 0·01 | 0·22 |
| CaO | 0·30 | 0·48 | 0·57 | 0·50 | 0·28 | 0·31 | MgO | 15·60 | 15·18 | 14·39 | 11·39 | 11·18 | CaO | 0·05 | 0·05 | 0·04 | 0·01 | 0·03 |
| Total | 99·69 | 100·54 | 99·72 | 100·75 | 99·69 | 99·39 | CaO | 0·00 | 0·00 | 0·03 | 0·01 | 0·03 | | | | | | |
| | | | | | | | Total | 100·71 | 99·72 | 100·33 | 99·01 | 101·73 | Total | 100·62 | 100·66 | 100·44 | 100·55 | 100·45 |
| O-basis | 12 | 12 | 12 | 12 | 12 | 12 | Si | 0·09 | 0·01 | 0·09 | 0·01 | 0·07 | | | | | | |
| Si | 3·04 | 3·03 | 3·02 | 3·00 | 2·97 | 3·01 | Al | 3·61 | 3·66 | 3·65 | 2·89 | 2·95 | O-basis | 5 | 5 | 5 | 5 | 5 |
| Al(T) | 2·02 | 2·02 | 2·01 | 2·01 | 1·97 | 1·98 | $Fe^{3+}$ | 0·20 | 0·33 | 0·17 | 1·09 | 0·91 | Si | 1·088 | 1·020 | 1·017 | 1·074 | 1·012 |
| $\sum$ | 5·06 | 5·05 | 5·03 | 5·01 | 4·97 | 5·01 | $Fe^{2+}$ | 0·87 | 0·80 | 0·95 | 1·01 | 1·12 | Al(T) | 1·847 | 1·965 | 1·964 | 1·894 | 1·935 |
| $Fe^{3+}$ | 0·00 | 0·00 | 0·00 | 0·00 | 0·03 | 0·02 | Mg | 1·22 | 1·21 | 1·14 | 0·99 | 0·94 | $\sum$ | 2·935 | 2·985 | 2·981 | 2·968 | 2·946 |
| $Fe^{2+}$ | 1·22 | 1·41 | 1·39 | 1·30 | 1·58 | 1·53 | Ca | 0·00 | 0·00 | 0·00 | 0·00 | 0·00 | $Fe^{3+}$ | 0·035 | 0·007 | 0·012 | 0·008 | 0·061 |
| Mg | 1·64 | 1·47 | 1·51 | 1·65 | 1·46 | 1·45 | Cations | 6·00 | 6·00 | 6·00 | 6·00 | 6·00 | Mg | 0·009 | 0·002 | 0·004 | 0·000 | 0·009 |
| $\sum$ | 2·86 | 2·88 | 2·91 | 2·95 | 3·08 | 3·00 | O-basis | 8·00 | 8·00 | 8·00 | 8·00 | 8·00 | Total | 2·970 | 2·992 | 2·993 | 2·976 | 3·008 |
| Total | 7·92 | 7·92 | 7·93 | 7·96 | 8·05 | 8·00 | $Fe^{3+}/FeT$ | 0·19 | 0·29 | 0·16 | 0·52 | 0·45 | | | | | | |
| $X_{Mg}$ | 0·57 | 0·51 | 0·52 | 0·56 | 0·48 | 0·49 | $X_{Mg}$ | 0·58 | 0·60 | 0·55 | 0·50 | 0·46 | | | | | | |

Spinels are $Fe^{3+}$ recalculated compositions. *n*, number of point analysis. Garnet analyses are included to illustrate the variation in composition and not the stoichiometry.

*Table 5: Representative chemical compositions of melt*

| Bulk: | M1 | | | M2 | | | M3 | | |
|---|---|---|---|---|---|---|---|---|---|
| $P$ (kbar): | 9 | 9 | 10 | 10 | 9 | 9 | 9 | 10 | 11 |
| $T$ (°C): | 900 | 1000 | 1050 | 1000 | 900 | 965 | 1100 | 1000 | 1000 |
| $n$: | 4 | 6 | 5 | 5 | 3 | 5 | 6 | 6 | 4 |
| $SiO_2$ | 72·45 | 73·77 | 73·85 | 73·65 | 69·98 | 71·96 | 71·93 | 73·15 | 72·63 |
| $Al_2O_3$ | 11·83 | 12·10 | 11·72 | 12·25 | 13·41 | 12·01 | 12·55 | 12·34 | 12·52 |
| FeO | 0·45 | 0·97 | 0·92 | 1·18 | 1·50 | 1·08 | 1·50 | 2·72 | 1·63 |
| MgO | 0·30 | 0·83 | 1·37 | 0·47 | 0·55 | 0·40 | 0·73 | 1·03 | 0·85 |
| CaO | 0·14 | 0·34 | 0·10 | 0·32 | 0·40 | 0·30 | 0·26 | 0·17 | 0·21 |
| $K_2O$ | 9·06 | 7·90 | 8·14 | 8·68 | 8·73 | 8·69 | 7·99 | 8·41 | 7·87 |
| Total | 94·23 | 95·92 | 96·11 | 96·56 | 94·57 | 94·43 | 94·96 | 97·80 | 95·70 |
| *CIPW normative mineralogy* | | | | | | | | | |
| Quartz | 40·12 | 45·50 | 45·27 | 41·89 | 38·61 | 40·96 | 44·02 | 43·20 | 45·14 |
| Orthoclase | 57·26 | 49·58 | 51·28 | 54·04 | 55·74 | 55·24 | 50·87 | 52·80 | 49·86 |
| Anorthite | 0·72 | 1·79 | 0·55 | 1·68 | 2·16 | 1·57 | 1·40 | 0·88 | 1·11 |
| Corundum | 1·90 | 3·12 | 2·90 | 2·40 | 3·49 | 2·23 | 3·70 | 3·12 | 3·89 |

$n$, number of point analysis.

scattering in earlier experiments was explained as due to 'overshooting' of the equilibrium composition (Ferry & Spear, 1978; Pattison & Newton, 1989; Carrington & Harley, 1995*a*).

Figure 7b shows the variation of ln $K_D^{Fe-Mg}$ (spinel–cordierite) vs temperature after correcting for $Fe^{3+}$ in spinel. The observed range in $K_D$ matches well with the natural data [reviewed by Kars *et al.* (1980)]. Vielzeuf (1983) calibrated an empirical spinel–cordierite thermometer based on natural occurrence data. This calibration is also plotted in Fig. 7b for comparison. Our regressed equation tallies well with that of Vielzeuf (1983).

We have plotted ln $K_D^{Fe-Mg}$ (Spr–Spl) vs temperature in Fig. 7c after correcting for $Fe^{3+}$ for both phases. The regressed equation has a similar slope to that empirically formulated by Owen & Greenough (1991). However, our experimental data show consistently lower estimates of ln $K_D$ for all the temperatures relative to the other formulation.

Fe–Mg partitioning between coexisting spinel and garnet is particularly interesting because earlier natural occurrence data (Sengupta *et al.*, 1991; Waters, 1991) and experimental data (Nichols *et al.*, 1992) have shown that the nature of partitioning may change as functions of pressure and bulk composition. The nature of partitioning determines the topology for equilibria involving both garnet and spinel, such as (Spr, Opx, Os, Bt), (Spr, Bt, Os, Crd) and (Crd, Bt, Os, Opx). The reactions shown in Fig. 1 have been deduced on the basis of the present experimental data, where garnet is more iron rich than coexisting spinel. This relationship remains valid within the bulk compositional range $X_{Mg}$ = 0·81–0·53, and within the $P$ range 9–12 kbar.

## PHASE RELATIONSHIPS

We now position the higher-pressure part of the KFMASH petrogenetic grid (Fig. 1) in $P$–$T$ space using the experimental data. The lower-pressure region related to the stability of osumilite + spinel assemblage has already been defined in $P$–$T$ space by Das *et al.* (2001). We adopt a 'pseudosection' approach and plot the experimental data for the three bulk compositions (Fig. 8a–c) and then construct isobaric $T$–$X$ sections (Fig. 9a–c) to discuss phase relationships (e.g. Carrington & Harley, 1995). High-variance fields in each of the pseudosections are designated. The three bulk compositions used in the experiments are designated as M1 ($X_{Mg}$ = 0·81), M2 ($X_{Mg}$ = 0·72) and M3 ($X_{Mg}$ = 0·53).

### High magnesian bulk composition, M1 (Fig. 8a)

Above 8·5 kbar, 900°C the entire $P$–$T$ window is occupied by orthopyroxene + sillimanite, but with different coexisting phases. Garnet makes its first appearance at 965°C, 10 kbar with orthopyroxene + sillimanite, and continues to be stable to 1000°C. However, it coexists

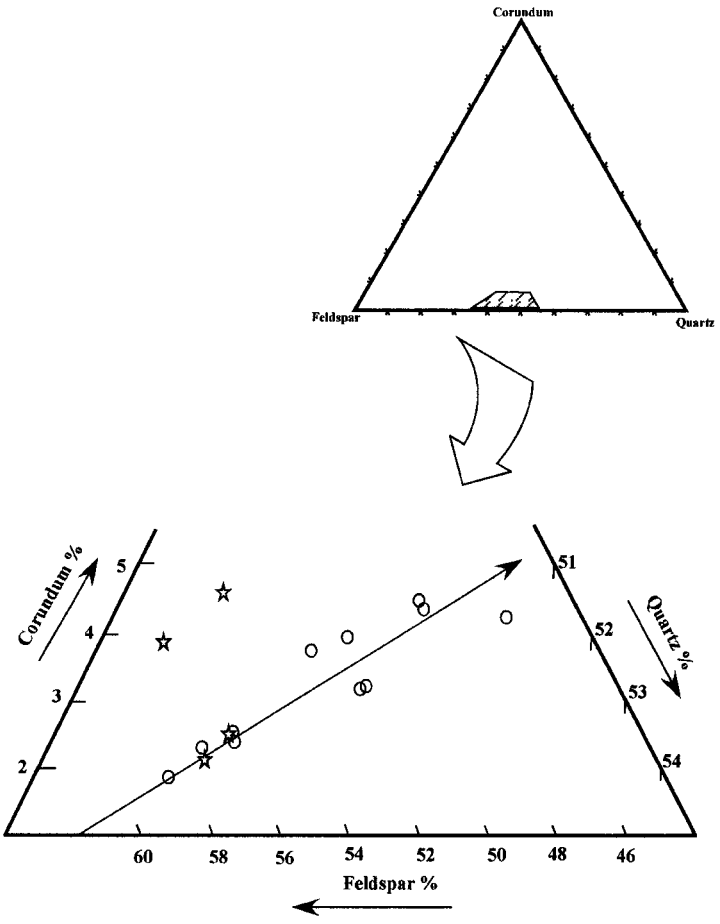


**Fig. 5.** Ternary plot for normative quartz–feldspar–corundum calculated from the melt compositions. Peraluminous granitic composition is evident from normative corundum. Arrow indicates the trend of probable potassium loss during analysis. ☆, data of Carrington & Harley (1995*a*).

with sapphirine + orthopyroxene + sillimanite at $T > 1000°C$, $P > 11$ kbar. Sapphirine is stable at $T > 950°C$, and coexists with orthopyroxene + sillimanite + spinel at 8–10 kbar and 1000–1100°C. Spinel + cordierite is stable with sapphirine and orthopyroxene at low pressures $< 9$ kbar, and $T > 1050°C$. The locations of (Crd,Bt,Os,Spr), (Crd,Bt,Os,Spl), (Crd,Bt,Os,Kfs), (Crd,Bt,Os,Sil) and (Crd,Bt,Os,Grt) are tightly constrained by close spaced runs. This results in stabilization of the invariant point [Crd,Bt,Os] with the assemblage Grt + Spr + Spl + Opx + Sil + Qtz + Kfs + Liquid at $P = 10$ kbar, $T = 1000°C$. At higher temperatures, the proportion of K-feldspar decreases whereas that of melt increases, leading to the stabilization of [Bt,Grt,Kfs] at $P = 8$ kbar, $T = 1000°C$.

## Intermediate magnesian bulk composition, M2 (Fig. 8b)

The major point to note is that all the invariant points move down pressure and slightly up temperature (the latter probably within the experimental uncertainty) with increase in bulk-rock $X_{Fe}$. This results in stabilization of garnet at lower pressures (as a result of the movement of [Crd,Bt,Os]) and of sapphirine (without garnet) to higher temperatures (as a result of the movement of [Crd,Grt,Bt]). The latter is consistent with natural observations that sapphirine stability is enhanced with increasing $X_{Mg}$ in the bulk composition. However, the assemblage sapphirine + garnet becomes stabilized relative to orthopyroxene + sillimanite at lower pressures. With lowering of $X_{Mg}$, the reaction (Spr,Grt,Crd,Os) moves up temperature, thereby increasing the stability of biotite + sillimanite + quartz to higher temperatures.

## Low magnesian bulk composition, M3 (Fig. 8c)

In this bulk composition sapphirine is not stabilized, consistent with previous experimental data (Audibert *et al.*, 1995) and with the observation that in nature

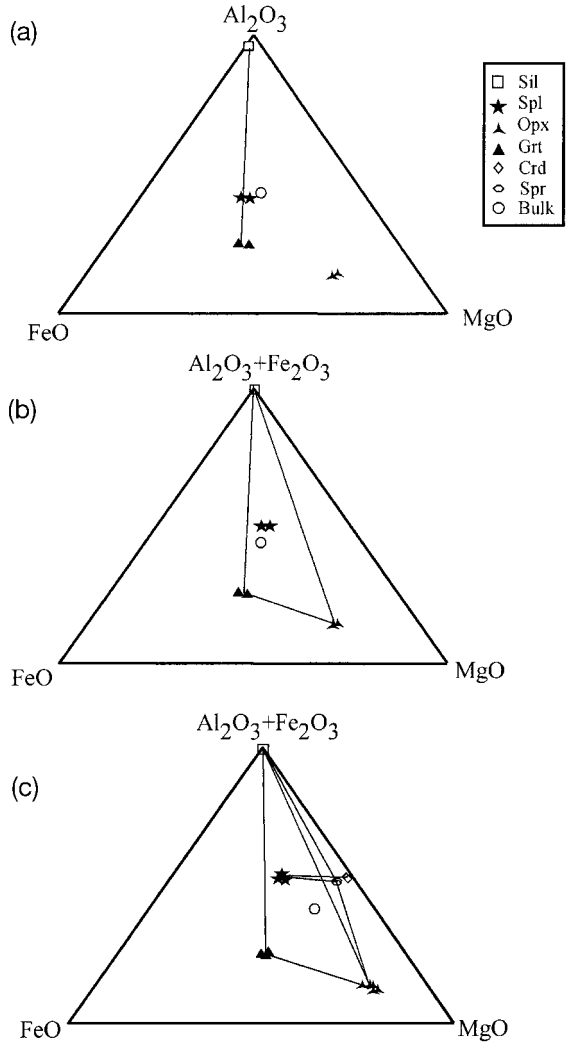


**Fig. 6.** (a) AFM plots projected from quartz, K-feldspar and melt for M3 at 10 kbar, 1100°C. (b) Same data plotted after $Fe^{3+}$ recalculation in ($Al_2O_3$ + $Fe_2O_3$)–FeO–MgO space. The movement of spinel compared with garnet, sillimanite and orthopyroxene should be noted. (c) AFM diagram projected from quartz, K-feldspar and melt for bulk composition M2 at 9 kbar, 1000°C and 8·5 kbar, 1050°C showing the reaction relation involving sapphirine.

sapphirine is found only in highly magnesian bulk compositions. This renders all the invariant points that involve sapphirine, e.g. [Crd,Bt,Os], [Crd,Grt,Bt] and [Grt,Bt,Kfs], metastable. Lowering of bulk-rock $X_{Mg}$ results in considerable widening of the stability of Fe-rich phases such as garnet and spinel and a wider stability field for Opx + Sil + Grt to pressures as low as 8·5 kbar and temperatures down to 900°C, as previously shown by Carrington & Harley (1995) at low $fO_2$. The spinel + cordierite + orthopyroxene assemblage becomes stable at lower pressures. Two crucial reactions, (Spr,Bt,Os,Spl) and (Spr,Bt,Os,Crd), define the invariant point [Spr,Bt,Os] at $T = 900$°C, $P = 8$ kbar. This invariant point is accessible to low magnesian bulk compositions, whereas [Crd,Bt,Os] is not 'seen' by this bulk composition. Das *et al.* (2001) suggested that [Spr,Grt,Bt] replaces [Crd,Bt,Grt] for this bulk composition.

## *T–X* diagrams

Phase relationships can also be portrayed in isobaric $T$–$X$ diagrams to understand the mineralogical variations as a function of pressure. The experimental data are plotted in three $T$–$X$ pseudosections at 7, 9 and 10 kbar (Fig. 9a–c). Increasing the pressure from 7 to 9 kbar causes disappearance of three high-variance fields, Os + Spl + Crd, Os + Opx + Spl and Bt + Crd + Kfs. Consequently, Bt + Sil + Kfs becomes stable to higher temperatures and its stability sweeps across to highly magnesian bulk compositions. There is no stability field for garnet-bearing assemblages at 7 kbar in any bulk composition. The Crd + Spl + Opx assemblage is stabilized only at relatively low magnesian bulk compositions and very high temperatures, and its thermal stability is expanded to lower temperatures at lower pressures. The result is consistent with experimental data in the system FMAS at high $fO_2$ (Annersten & Seifert, 1981). Thus, this assemblage is diagnostic of low-pressure–high-temperature metamorphism. The assemblage Opx + Spl + Sil becomes stable at 9 kbar over a wide bulk compositional range at temperatures >900°C. Sapphirine-bearing assemblages (Spr + Crd + Opx and Spr + Opx + Spl) become stable at lower temperatures with increase in pressure from 7 to 9 kbar (Fig. 6c). Garnet is not stable at 7 kbar within the investigated compositional range, which contrasts with the observation at low $fO_2$. Further increase in pressure to 10 kbar (Fig. 9c) causes an expansion in the stability field of Opx + Spl + Sil to higher temperatures, and consequently up-temperature shifting of the field of Spr + Opx + Sil. There is a significant increase in the stability field of garnet-bearing assemblage (Grt + Opx + Sil) to higher temperatures, thereby eliminating the field of Crd + Spl + Opx. Sapphirine–garnet coexistence is permitted at 10 kbar in the M2 bulk composition at $T = 1050$°C, which is stable only at higher pressures in the M1 bulk composition. This implies shifting of the Spr + Grt stability field to higher pressures with increasing $X_{Mg}$ in the bulk composition.

Based on these results, some of the invariant points in Fig. 1 can be positioned in $P$–$T$ space to develop a petrogenetic grid in the system KFMASH at high $fO_2$ (Fig. 10). The invariant points [Spr,Grt,Opx], [Spr,Grt,Crd], [Crd,Grt,Bt] and [Bt,Grt,Kfs] are taken from Das *et al.* (2001). [Spr,Grt,Crd] is tightly

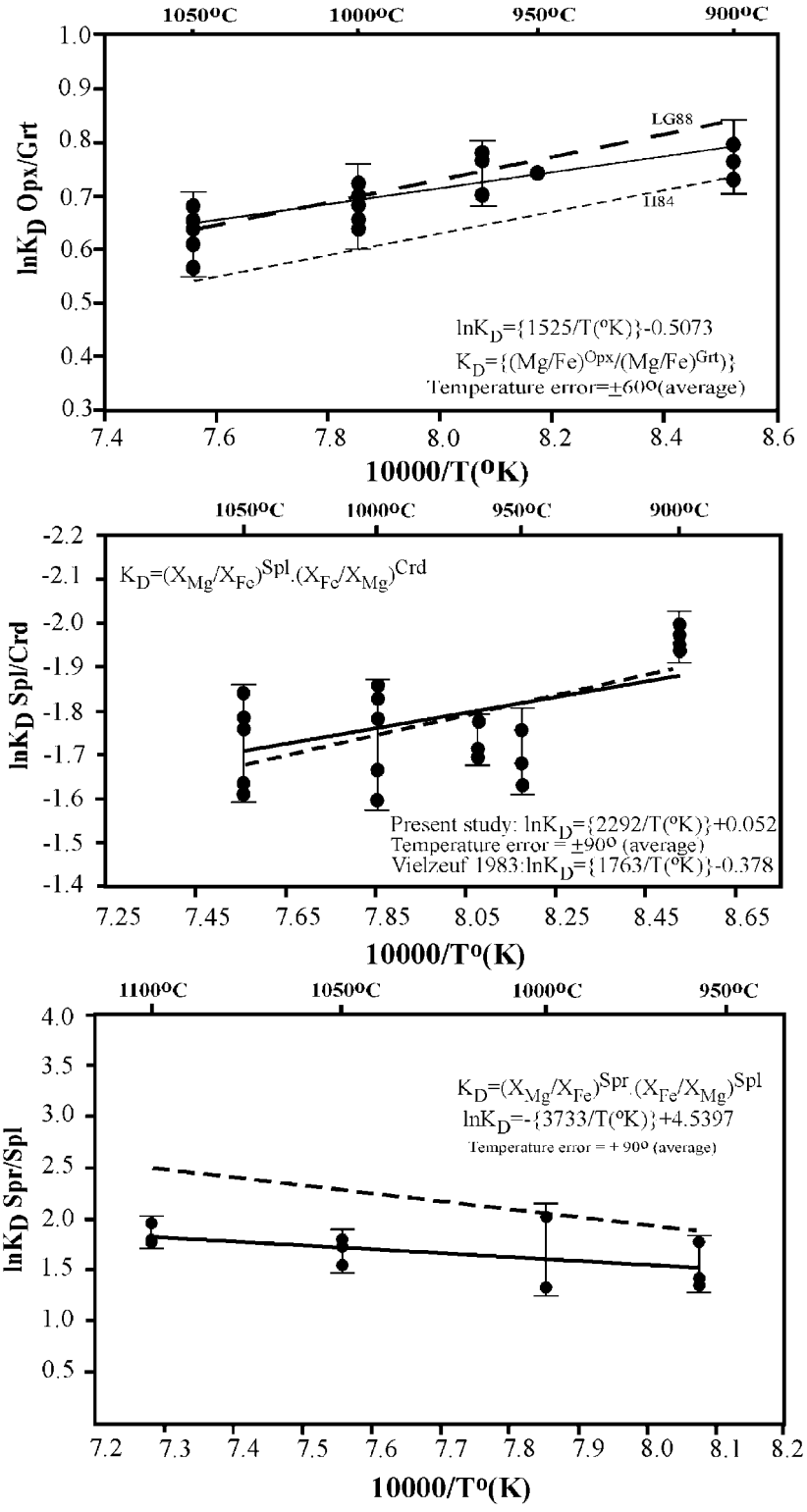


**Fig. 7.** (a) ln $K_D$ vs $1/T$ (K) plot for coexisting orthopyroxene and garnet. Data calculated from Lee & Ganguly (1988) (LG88; bold dashed line at 12 kbar) and Harley (1984) (H84; fine dashed line at 12 kbar) have also been plotted for comparison. (b) ln $K_D$ vs $1/T$ (K) plot of all coexisting spinel–cordierite. The dashed line is the approximate linear trend from this study and the continuous line represents that from the formulation of Vielzeuf (1983). (c) ln $K_D$ vs $1/T$ (K) plot for coexisting sapphirine and spinel. The continuous line represents the linear trend from the data of these experiments and the dashed line that from the empirical equation by Owen & Greenhough (1991).

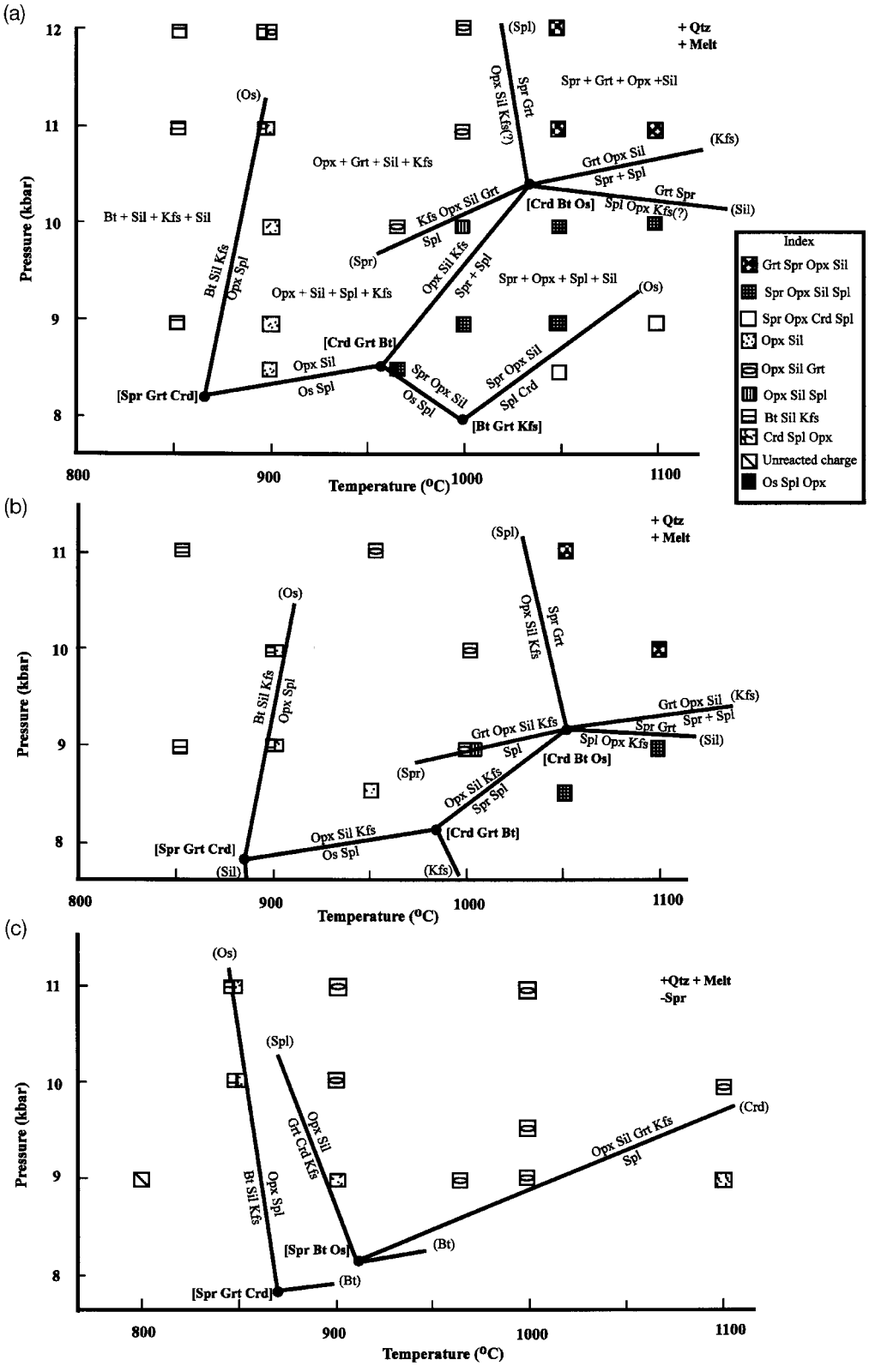


**Fig. 8.** $P$–$T$ pseudosections for the three bulk compositions used in the experiments. Mineral assemblages for each run product are shown. (a) For $X_{Mg} = 0{\cdot}81$; (b) for $X_{Mg} = 0{\cdot}72$; (c) for $X_{Mg} = 0{\cdot}53$.

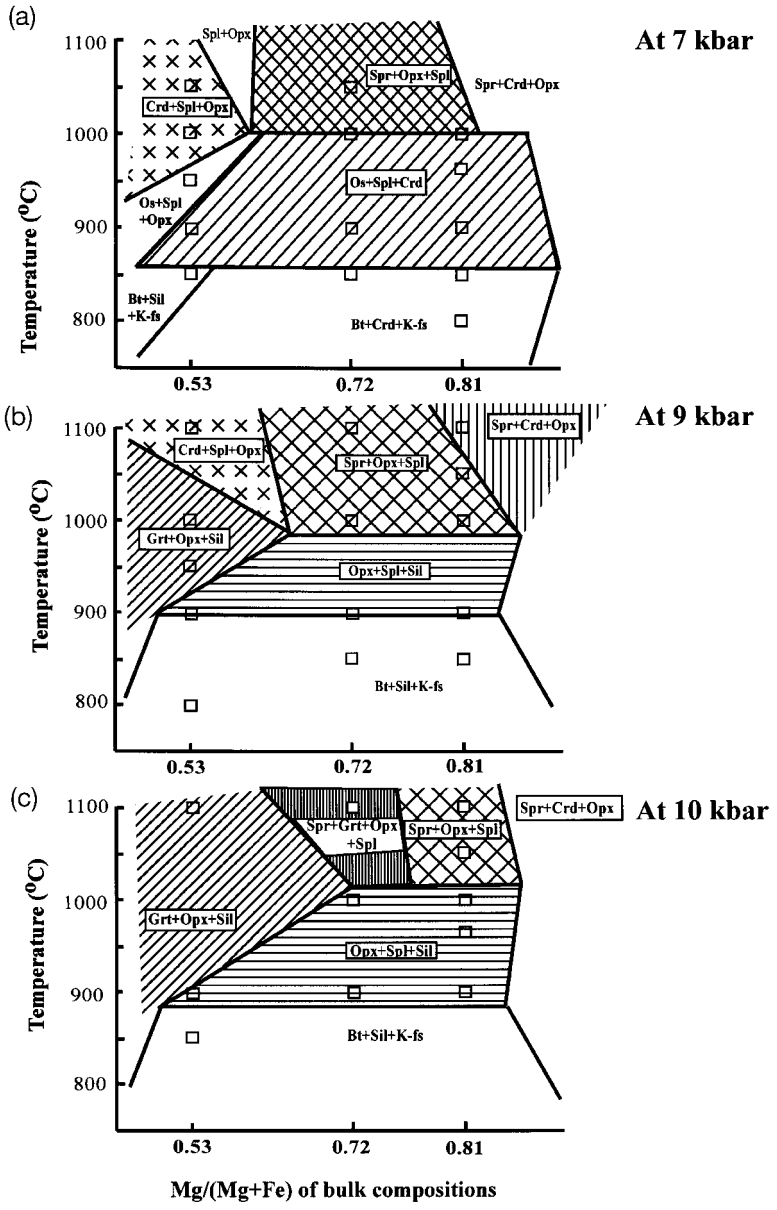


**Fig. 9.** *T*–*X* diagrams at (a) 7 kbar, (b) 9 kbar and (c) 10 kbar. Quartz and liquid are additional phases. The *X*-axis is not to scale. The data points for (a) are from Das *et al.* (2001).

constrained by the appearance of osumilite on the low-temperature side, and is placed at 8–8·2 kbar and 850–865°C. Likewise, disappearance of osumilite in the runs on the high-temperature side locates [Crd,Grt,Bt] at 8–8·5 kbar and 965°C. [Bt,Grt,Kfs] is constrained by appearance of spinel + cordierite + orthopyroxene with or without sapphirine, and disappearance of K-feldspar, and is located at 8 kbar, 1000°C. The location of [Crd,Bt,Os] is problematic because lowering of $X_{Mg}$ in the bulk composition moves it up temperature and down pressure (Fig. 8a and b). Moreover, non-appearance of sapphirine in the lowest magnesian bulk composition renders this invariant point inaccessible. However, in the bulk compositions M1 and M2, its position is tightly constrained by runs on both sides of the equilibria (Crd,Bt,Os,Spr), (Crd,Bt,Os,Spl) and (Crd,Bt,Os,Grt) (Fig. 8a and b). On the basis of available data, [Crd,Bt,Os] is best located between 9 and 10 kbar, 900°C and 1000°C. In the lowest magnesian bulk composition [Spr,Bt,Os] can be located at 8 kbar,

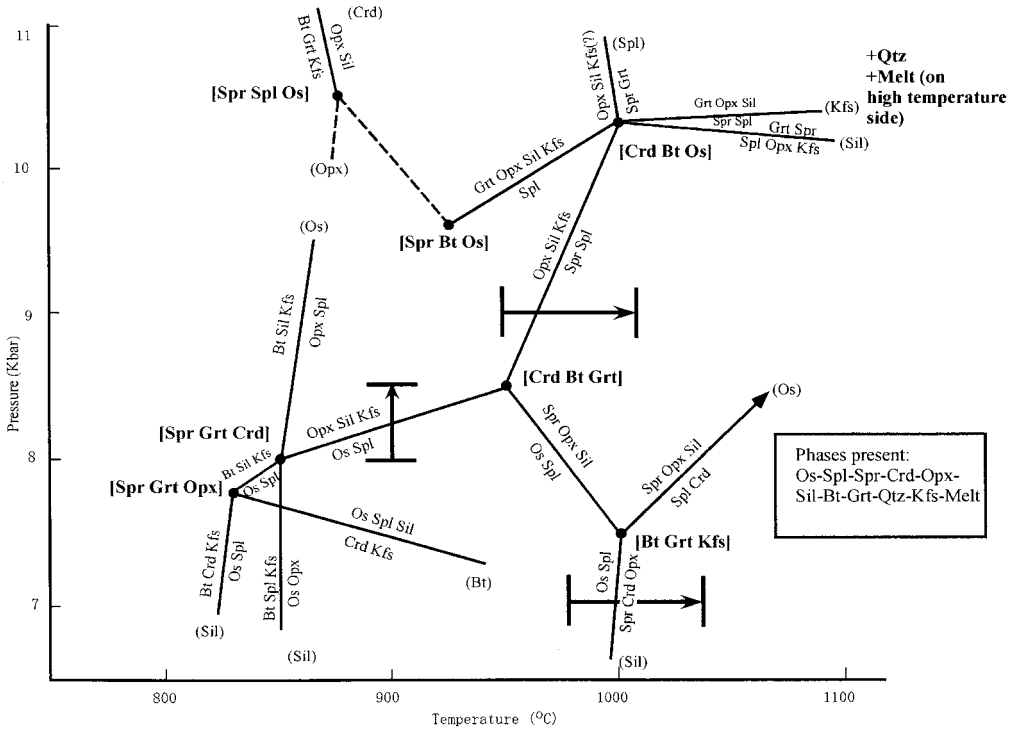


**Fig. 10.** Experimentally determined $P$–$T$ petrogenetic grid in the system KFMASH at high $fO_2$ (near HM buffer) showing univariant equilibria. The arrows show the $P$–$T$ reversal bracket.

900°C because of the constraint imposed by (Spr,Bt,Os,Spl) and (Spr,Bt,Os,Crd). The invariant point [Spr,Spl,Os] is located at 900°C, 9 kbar at low $fO_2$ (Carrington & Harley, 1995). Garnet appears in the biotite-melting interval at 12 kbar, 900°C in M1 and at 10 kbar, 900°C in M3 composition. Both are related to the reaction (Spr,Spl,Os,Crd), which is located on the high-pressure side of [Spr,Spl,Os] (Fig. 1). In the M3 bulk composition, the reaction (Spr,Spl,Os,Bt), which occurs on the lower-pressure side of [Spr,Spl,Os], is intersected at 900°C, 9 kbar. Taking all three into consideration, we locate [Spr,Spl,Os] at 900°C, 9–10 kbar. This is in excellent agreement with the experimental results at low $fO_2$ (Carrington & Harley, 1995). This invariant point is supposed to be independent of $fO_2$ (Hensen & Harley, 1990).

## APPLICATION OF THE PETROGENETIC GRID TO SOME NATURAL OCCURRENCES

Morse & Talley (1971) reported a high $fO_2$ sapphirine–quartz–orthopyroxene–spinel–sillimanite-bearing assemblage from Wilson Lake area, central Labrador, Canada. This occurrence had sapphirine, spinel (hercynitic), orthopyroxene, sillimanite, quartz, magnetite and corundum. Textural features in this rock indicate formation of orthopyroxene + sillimanite from sapphirine + spinel + quartz. Those workers explained the textural evolution as due to cooling from 1350°C, 13 kbar. Our experimental data indicate that this reaction (Crd,Bt,Os,Grt) is intersected as a result of cooling from $T \sim 1000$°C, but at pressures below 9–10 kbar (depending on the bulk-rock $X_{Mg}$), i.e. below the invariant point [Crd,Bt,Os] (Fig. 11, path 4). At higher pressures, garnet would have appeared in the assemblage. A similar mineral assemblage and texture were reported by Caporuscio & Morse (1978) from Salt Hill, Peekskill, New York, where those workers qualitatively predicted cooling from very high temperatures at pressures $<9{\cdot}5$ kbar. Total absence of garnet and cordierite in this rock constrains peak $P$–$T$ conditions in this area bounded by the reaction (Bt,Grt,Kfs,Os) and the invariant point [Crd,Bt,Os], i.e. 8–10 kbar, $T > 900$–1000°C, depending on bulk-rock $X_{Mg}$ (Fig. 11, path 5). The textural feature can also be explained by cooling across (Crd,Bt,Os,Grt).

Kars *et al.* (1980) and Tobi *et al.* (1985) described both osumilite-bearing and osumilite-free assemblages from Rogaland, southern Norway. The rocks are polymetamorphic and mineral chemical data reported by

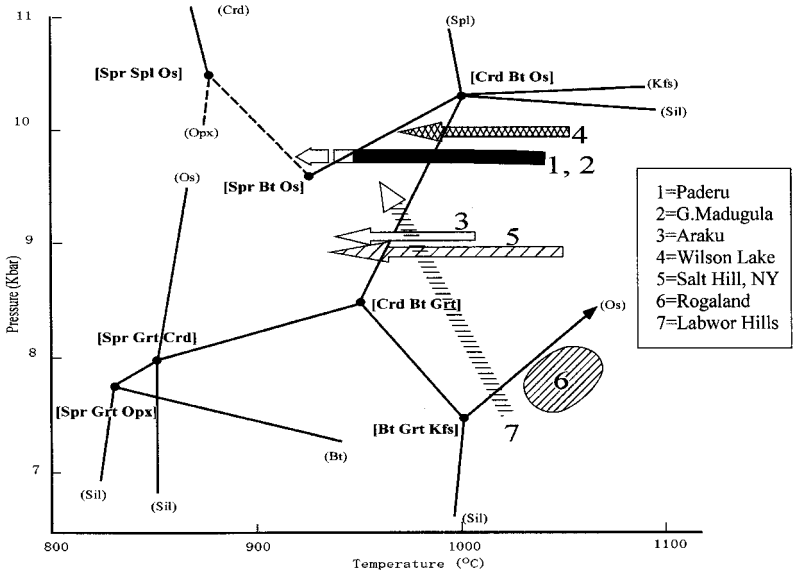


**Fig. 11.** $P$–$T$ trajectories (with arrows) and pressure–temperature conditions of metamorphism of seven natural occurrences discussed in the text. 1, Paderu: Lal *et al.* (1987); 2, Gangaraja Madugula: Mohan *et al.* (1997); 3, Araku: Sengupta *et al.* (1991); 4, Wilson Lake: Morse & Talley (1971); 5, Salt Lake, NY: Caporuscio & Morse (1978); 6, Rogaland: Kars *et al.* (1980), Tobi *et al.* (1985); 7, Labwor Hills: Sandiford *et al.* (1987).

those workers suggest local variations in bulk chemistry. Osumilite-bearing assemblages were interpreted by Das *et al.* (2001) to have stabilized below 8 kbar, and $T \sim 1000°C$. Most of the samples are Fe rich and contain the assemblage cordierite + spinel + orthopyroxene. This assemblage is stable below 9 kbar, but at $T > 1000°C$, according to the present experimental data (Fig. 8c). In one sample sapphirine coexists with orthopyroxene + spinel + cordierite, presumably in higher magnesian bulk composition. The present experimental data (Fig. 8a and b) for higher magnesian bulk composition also constrain this assemblage at $T \sim 1000°C$. Therefore, both the osumilite-bearing and osumilite-free assemblages from this locality attest to identical $P$–$T$ conditions from our experimental data (Fig. 11, path 6).

Sandiford *et al.* (1987) described sapphirine from Labwor Hills, Uganda, not only as a breakdown product of osumilite [discussed by Das *et al.* (2001)], but also as part of an early stabilized spinel–ilmenohaematite–magnetite–cordierite–quartz–sapphirine assemblage. Reaction textures indicate the reaction

$$\text{spinel} + \text{cordierite} = \text{sapphirine} + \text{orthopyroxene} + \text{sillimanite (Os,Grt,Kfs,Bt)}.$$

This is followed by the reaction

$$\text{sapphirine} + \text{spinel} + \text{quartz} = \text{orthopyroxene} + \text{sillimanite (Os,Bt,Grt,Crd)}.$$

According to the petrogenetic grid (Fig. 10), these two reactions are successively intersected by movement across (Os,Grt,Kfs,Bt) as a result of an increase in pressure, and (Os,Bt,Crd,Grt) as a result of cooling from peak conditions. Alternatively, both reactions can be intersected by loading during cooling, as suggested by Sandiford *et al.* (1987). Peak $P$–$T$ conditions of 9–10 kbar, 1000°C, predicted by the grid, and the trajectory are in close agreement with those predicted by Sandiford *et al.* independently (Fig. 11, path 7).

Several occurrences of high Mg–Al granulites equilibrated at high $fO_2$, indicated by oxide mineralogy, have been reported from the Eastern Ghats Belt, India. At Paderu the metamorphic history of assemblages with pre-existing osumilite (Lal *et al.*, 1987) has been discussed by Das *et al.* (2001). Lal *et al.* (1987) also described assemblages where osumilite was never stabilized, presumably because of lower magnesian bulk composition. Textural features suggest formation of orthopyroxene + sillimanite ± garnet at the expense of sapphirine and spinel. This can occur because of movement across (Os,Crd,Grt,Bt) and (Os,Crd,Bt,Spr) as a result of cooling from $T > 1000°C$ within 9–10 kbar pressure (Fig. 11, path 1). Although the $P$–$T$ estimates are close to that predicted by Lal *et al.* (1987), the deduced trajectory is not.

Similar textural features indicating formation of orthopyroxene + sillimanite, followed by garnet, at the expense of sapphirine and spinel have been reported by Mohan *et al.* (1997) from Gangaraja

Madugala. This can also be explained by a cooling trajectory across (Crd,Bt,Os,Grt) and (Crd,Bt,Os,Spr) from ultrahigh temperatures (Fig. 11, path 2). Sengupta *et al.* (1991) described two sapphirine-free assemblages from Araku in bulk compositions that perfectly match with our experiments on the M3 composition. In these rocks, orthopyroxene + sillimanite and garnet + sillimanite appeared from spinel + quartz. Both the divariant reactions can be associated with the KFMASH univariant reaction (Crd,Bt, Os,Spr), which would indicate cooling from $T > 950°C$, between 8 and 9 kbar (Fig. 11, path 3). This tallies very well with independent estimation of Sengupta *et al.* (1991).

## CONCLUDING REMARKS

Das *et al.* (2001) have shown that the osumilite + spinel assemblage should be a characteristic high-$T$–low-$P$ assemblage in high Mg–Al granulites metamorphosed at high $fO_2$, and could conceivably be the early stabilized assemblage in similar rocks metamorphosed along a counterclockwise $P$–$T$ trajectory. The present experimental data indicate further that spinel + cordierite + orthopyroxene should be a diagnostic high $fO_2$ assemblage of very high-temperature–low-pressure regional or contact metamorphism of relatively Fe-rich rocks. In more magnesian bulk composition, sapphirine joins the assemblage. Sapphirine + cordierite + orthopyroxene will be the extreme high-temperature assemblage at higher pressures only for highly magnesian rocks. These assemblages will be stabilized early in rocks metamorphosed under a counterclockwise $P$–$T$ path, and late along a clockwise $P$–$T$ path. There is a limited stability field for the sapphirine + garnet + orthopyroxene assemblage at higher pressures. This assemblage is stabilized within a narrow bulk compositional range at pressures $>10$ kbar and temperatures $>1000°C$. Stability of garnet is extended to lower pressures with increasing Fe-rich bulk composition at high $fO_2$ in the assemblage garnet + orthopyroxene + spinel, which is a characteristic high-temperature assemblage at pressures $>9$ kbar, but for highly magnesian bulk compositions. The orthopyroxene + spinel + sillimanite assemblage is stable within a $P$–$T$ window of 8–10 kbar, 900–1000°C. The present experimental data therefore help to identify characteristic mineral assemblages that are likely to be stable in high Mg–Al granulites as functions of $P$–$T$–$X_{Mg}$ and at high $fO_2$. As discussed by Das *et al.* (2001), these $P$–$T$ windows will move up pressure and up temperature because of incorporation of Zn in spinel and F and Ti in biotite in natural rocks. Despite this, the derived petrogenetic grid is consistent with the $P$–$T$ conditions and $P$–$T$ trajectories deduced from several natural occurrences of high Mg–Al granulites at high $fO_2$.

## ACKNOWLEDGEMENTS

We thank Professors Bas J. Hensen, Simon Harley and M. Arima for fruitful discussion and suggestion at various stages of the work. K.D. is also indebted to Professor K. Fujino, Professor T. Kikuchi, Professor M. Yoshida, Dr N. Miyajima, Dr T. Shinmei and Dr N. Tomioka for their constant support. K.D. thanks Mr S. Terada, the technical officer of Hokkaido University, for assisting during the experiments. K.D. was supported by a Japanese Government scholarship during this work. S.D. was supported by the annual research grant of Monbusho towards defraying travel expenses. S.D. is particularly grateful to Dr Pulak Sengupta for many constructive suggestions and invigorating discussions over the last 15 years related to ultrahigh-temperature granulites. We acknowledge with thanks some useful tips given by Professors Sumit Chakraborty and T. Oba regarding experimental procedure. We thank Dr P. McDade and Professor S. L. Harley for their constructive suggestions on an earlier version of the manuscript.

## REFERENCES

Annersten, H. & Seifert, F. (1981). Stability of the assemblage orthopyroxene–sillimanite–quartz in the system MgO–FeO–$Fe_2O_3$–$Al_2O_3$–$SiO_2$–$H_2O$. *Contributions to Mineralogy and Petrology* **77**, 158–165.

Arima, M. (1978). Phase equilibria in the system $MgSiO_3$–$Al_2O_3$–$Fe_2O_3$ at high temperatures and pressures, with special reference to the solubility of $Al_2O_3$ and $Fe_2O_3$ in enstatite. *Journal of Faculty of Science, Hokkaido University, Series IV* **18**(3), 305–338.

Arima, M. & Gower, C. F. (1991). Osumilite-bearing granulites in the eastern Grenville Province, eastern Labrador, Canada: mineral parageneses and metamorphic conditions. *Journal of Petrology* **32**, 29–62.

Audibert, N., Hensen, B. J. & Bertrand, P. (1995). Experimental study of phase relations involving osumilite in the system $K_2O$–FeO–MgO–$Al_2O_3$–$SiO_2$–$H_2O$ at high pressure and temperature. *Journal of Metamorphic Geology* **13**, 331–344.

Bohlen, S. R. & Boettcher, A. L. (1982). The quartz–coesite transformation: a precise determination and the effects of other components. *Journal of Geophysical Research* **87**(B8), 7073–7078.

Bose, S., Fukuoka, M., Sengupta, P. & Dasgupta, S. (2000). Evolution of high Mg–Al granulites from Sunkarimetta, Eastern Ghats, India: evidence for a lower crustal heating–cooling trajectory. *Journal of Metamorphic Geology* **18**, 223–240.

Boyd, F. R. & England, J. L. (1960). Apparatus for phase equilibrium measurements at pressures up to 50 kbar and temperatures up to 1350°C. *Journal of Geophysical Research* **65**, 741–748.

Caporuscio, F. A. & Morse, S. A. (1978). Occurrence of sapphirine plus quartz at Peekskill, New York. *American Journal of Science* **278**, 1334–1342.

Carrington, D. P. & Harley, S. L. (1995*a*). Partial melting and phase relations in high-grade metapelites: an experimental petrogenetic grid in the KFMASH system. *Contributions to Mineralogy and Petrology* **120**, 270–291.

Carrington, D. P. & Harley, S. L. (1995*b*). The stability of osumilite in metapelitic granulites. *Journal of Metamorphic Geology* **13**, 613–625.

Clarke, S. P., Jr (1959). Effect of pressure on the melting points of eight alkali halides. *Journal of Chemical Physics* **31**, 1526–1531.

Das, K., Dasgupta, S. & Miura, H. (2001). Stability of osumilite coexisting with spinel solid solution in metapelitic granulite at high oxygen fugacity. *American Mineralogist* **86**, 1423–1434.

Dasgupta, S., Sengupta, P., Ehl, J., Raith, M. & Bardhan, S. (1995). Reaction textures in a suite of spinel granulites from the Eastern Ghats Belt, India: evidence for polymetamorphism, a partial petrogenetic grid in the system KFMASH and the roles of ZnO and $Fe_2O_3$. *Journal of Petrology* **36**, 435–461.

Dasgupta, S., Ehl, J., Raith, M., Sengupta, P. & Sengupta, P. R. (1997). Mid-crustal contact metamorphism around the Chirmakurthy mafic–ultramafic complex, Eastern Ghats belt, India. *Contributions to Mineralogy and Petrology* **129**, 182–197.

Ellis, D. J., Sheraton, J. W., England, R. N. & Dallwitz, W. B. (1980). Osumilite–sapphirine–quartz granulites from Enderby Land, Antarctica—mineral assemblages and reactions. *Contributions to Mineralogy and Petrology* **72**, 123–143.

Ferry, J. M. & Spear, F. S. (1978). Experimental calibration of the partitioning of Fe and Mg between biotite and garnet. *Contributions to Mineralogy and Petrology* **66**, 113–117.

Grant, J. A. (1985). Phase-equilibria in low-pressure partial melting of pelitic rocks. *American Journal of Science* **285**, 409–435.

Grew, E. S. (1982). Sapphirine, kornerupine and sillimanite orthopyroxene in the charnockitic region of south India. *Journal of the Geological Society of India* **23**, 469–505.

Hariya, Y. & Fukunaga, O. (1969). Glass-cell in high temperature–high pressure experiments, *Ceramics* **4**(9), 758–764.

Harley, S. L. (1984). An experimental study of the partitioning of Fe and Mg between garnet and orthopyroxene. *Contributions to Mineralogy and Petrology* **86**, 359–373.

Harley, S. L. (1989). The origins of granulites: a metamorphic perspective. *Geological Magazine* **126**, 215–247.

Harley, S. L. (1998). On the occurrences and characterization of ultrahigh-temperature crustal metamorphism. In: Treloar, P. J. & O'Brien, P. J. (eds) *What Drives Metamorphism and Metamorphic Reactions? Geological Society, London, Special Publications* **138**, 81–108.

Harley, S. L. & Motoyoshi, Y. (2000). Al zoning in orthopyroxene in a sapphirine quartzite: evidence for >1120°C UHT metamorphism in the Napier Complex, Antarctica, and implications for the entropy of sapphirine. *Contributions to Mineralogy and Petrology* **138**, 293–207.

Hensen, B. J. (1971). Theoretical phase relations involving cordierite and garnet in the system $MgO–FeO–Al_2O_3–SiO_2$. *Contributions to Mineralogy and Petrology* **33**, 191–214.

Hensen, B. J. (l986). Theoretical phase relations involving garnet and cordierite revisited: the influence of oxygen fugacity on the stability of sapphirine and spinel in the system Mg–Fe–Al–Si–O. *Contributions to Mineralogy and Petrology* **92**, 191–214.

Hensen, B. J. & Green, D. H. (1971). Experimental study of cordierite and garnet in pelitic compositions at high pressures and temperatures I: compositions with excess alumino-silicate. *Contributions to Mineralogy and Petrology* **33**, 309–330.

Hensen, B. J. & Harley, S. L. (1990). Graphical analysis of $P$–$T$–$X$ relations in granulite facies metapelites. In: Ashworth, J. R. & Brown, M. (eds) *High Temperature Metamorphism and Crustal Anatexis*. London: Unwin Hyman, pp. 19–56.

Higgins, J. B., Ribbe, P. H. & Herd, R. K. (1979). Sapphirine I. Crystal chemical contributions. *Contributions to Mineralogy and Petrology* **68**, 349–356.

Iiyama, T., Kawamura, K. & Nakashima, S. (1994). *Experimental Geochemistry*. Tokyo: University of Tokyo Press, pp. 47–50.

Kamineni, D. C. & Rao, A. T. 1988. Sapphirine granulites from Kakanuru area, Eastern Ghats, India. *American Mineralogist* **73**, 692–700.

Kars, H., Jansen, B. H., Tobi, A. C. & Poorter, R. P. E. (1980). The metapelitic rocks of the polymetamorphic Precambrian of Rogaland, SW Norway, Part II. Mineral relations between cordierite, hercynite and magnetite within the osumilite-in isograd. *Contributions to Mineralogy and Petrology* **74**, 235–244.

Kretz, R. (1983). Symbols for rock-forming minerals. *American Mineralogist* **68**, 277–279.

Lal, R. K., Ackermand, D. & Upadhyay, H. (1987). $P$–$T$–$X$ relationships deduced from corona textures in sapphirine–spinel–quartz assemblages from Paderu, southern India. *Journal of Petrology* **28**, 1139–1168.

Lee, H. Y. & Ganguly, J. (1988). Equilibrium compositions of coexisting: garnet and orthopyroxene: experimental determinations in the system $FeO–MgO–Al_2O_3–SiO_2$, and applications. *Journal of Petrology* **29**(1), 93–114.

McDade, P. & Harley, S. L. (2001). A petrogenetic grid for aluminous granulite facies metapelites in the KFMASH system. *Journal of Metamorphic Geology* **19**, 45–59.

Mohan, A., Tripathy, P. & Motoyoshi, Y. (1997). Reaction history of sapphirine granulites and a decompressional $P$–$T$ path in a granulite complex from the Eastern Ghats. *Proceeding of Indian Academy of Science (Earth and Planetary Science)* **106**, 115–129.

Morse, S. A. & Talley, J. H. (1971). Sapphirine reactions in deep-seated granulites near Wilson Lake, Central Labrador, Canada. *Earth and Planetary Science Letters* **10**, 325–328.

Newton, R. C. (1972). An experimental determination of the high pressure stability limits of magnesian cordierite under wet and dry conditions. *Journal of Geology* **80**, 398–420.

Nichols, G. T., Berry, R. F. & Green, D. H. (1992). Internally consistent gahnitic spinel–cordierite–garnet equilibria in the FMASHZn system: geothermobarometry and applications. *Contributions to Mineralogy and Petrology* **111**, 362–377.

Nixon, P. H., Reedman, A. J. & Burns, L. K. (1973). Sapphirine-bearing granulites from Labwor, Uganda. *Mineralogical Magazine* **39**, 420–428.

Nowicki, T. E., Frimmel, H. E. & Waters, D. J. (1995). The occurrence of osumilite in pelitic granulite of the Namaqualand Metamorphic Complex, South Africa. *South African Journal of Geology* **98**(2), 191–201.

Owen, J. V. & Greenough, J. D. (1991). An empirical sapphirine–spinel Mg–Fe exchange thermometer and its application to high grade xenoliths in the Popes Harbour dyke, Nova Scotia, Canada. *Lithos* **26**, 317–332.

Patiño Douce, A. E. & Johnston, A. D. (1991). Phase equilibria and melt productivity in the pelitic system: implication for the origin of peraluminous granitoids and aluminous granulites. *Contributions to Mineralogy and Petrology* **107**, 202–218.

Pattison, D. R. M. & Newton, R. C. (1989). Reversed experimental calibration of the garnet–clinopyroxene Fe–Mg exchange thermometer. *Contributions to Mineralogy and Petrology* **101**, 87–103.

Sandiford, M., Neall, F. B. & Powell, R. (1987). Metamorphic evolution of aluminous granulites from Labwor Hills, Uganda. *Contributions to Mineralogy and Petrology* **95**, 217–225.

Sengupta, P., Karmakar, S., Dasgupta, S. & Fukuoka, M. (1991). Petrology of spinel granulites from Araku, Eastern Ghats, India,

and a petrogenetic grid for sapphirine-free rocks in the system FMAS. *Journal of Metamorphic Geology* **9**, 451–459.

Tobi, A. C., Hermans, G. A. E. M., Maijer, C. & Jansen, J. B. H. (1985). Metamorphic zoning in the high-grade Proterozoic of Rogaland–Vest Agder, SW Norway. In: Tobi, A. C. & Touret, J. L. R. (eds) *The Deep Proterozoic Crust in the North Atlantic Provinces, NATO ASI Series C158*. Dordrecht: D. Reidel, pp. 477–497.

Vielzeuf, D. (1983). The spinel and quartz associations in high grade xenoliths from Tallante (SE Spain) and their potential use in geothermometry and barometry. *Contributions to Mineralogy and Petrology* **82**, 301–311.

Waters, D. J. (1989). Metamorphic evidence for the heating and cooling path of Namaqualand granulites. In: Daly, J. S., Cliff, R. A. & Yardley, B. W. D. (eds) *Evolution of Metamorphic Belts. Geological Society, London, Special Publications* **43**, 357–363.

Waters, D. J. (1991). Hercynite–quartz granulites: phase relations and implications for crustal processes. *European Journal of Mineralogy* **3**, 367–386.